Development of Adapted Capacitance Manometer for Thermospheric Applications

Cameron S. Orr

Thesis submitted to the Faculty of the
Virginia Polytechnic Institute and State University
in partial fulfillment of the requirements for the degree of

Master of Science
in
Electrical Engineering

Gregory D. Earle, Chair
Dan Sable
Dennis Sweeney

April 15, 2015
Blacksburg, Virginia

Keywords: Capacitance Manometer, Instrument Development, Space Instrumentation,
Pressure Instrument, Vacuum Testing

Development of Adapted Capacitance Manometer for Thermospheric Applications

Cameron S. Orr

ABSTRACT

An adapted capacitance manometer is a sensor composed of one fixed plate and one movable plate that is able to make accurate pressure measurements in a low pressure environment. Using detection circuitry, a change in capacitance between the two plates can be measured and correlated to a differential pressure. First, a high sensitivity manometer is produced that exhibits a measurable change in capacitance when experiencing a pressure differential in a low pressure space environment. Second, an accurate and precise detection circuit is identified to measure the change in capacitance. Both, the manometer and the detection circuitry, are tested separately and together to confirm accurate measurements when experiencing small pressure differentials. The manometer shows low sensitivity at the desired differential pressure range but reacts predictably when compared to simulations. The manometer also shows an unexpected correlation in capacitance change to temperature change.

Development of Adapted Capacitance Manometer for Thermospheric Applications

Cameron S. Orr

GENERAL ABSTRACT

For space environment pressure measurements, there are few low-power instruments readily available. An adapted capacitance manometer is a low-power electrical device that uses the physical properties of a capacitor to measure pressure waves, particularly pressure waves with very small amplitudes. A circuit designed to measure a changing capacitance is used to correlate a changing capacitance with a pressure wave acting on an adapted capacitance manometer. From empirical testing, the adapted capacitance manometers developed for this research show low sensitivity to pressure changes but react consistently. These findings could be built upon to continue development of a low-power pressure instrument suitable for space environments.

Dedication

To my parents, Gary and Martha Orr for their continual support and encouragement.

Acknowledgments

I would like to thank the Virginia Space Grant Association for supporting my research through the Graduate STEM Research Fellowship Program. I would also like to give special thanks to Dr. Greg Earle for his guidance on this project. This work could not have been completed without the efforts of Dr. Jeong Bong Lee and Jun Hyeon Yoo at the University of Texas at Dallas in developing and producing the capacitance manometer. Additional thanks go to Matthew Francom for performing simulations presented in this work, Daniel Martin for assembly of the vacuum chamber, Dennis Crump for software development, Stephen Noel for aid in software debugging, and Lee Kordella for his help with manometer test fixture assembly.

Funding for this research provided by the National Aeronautics and Space Administration (NNX12AF30G).

Unless otherwise noted, all photos by author, 2016.

Contents

List of Figures

List of Tables

Chapter 1

Introduction

The adaptive capacitance manometer is a low power instrument designed to measure pressure fluctuations in the ionosphere and thermosphere. The team developing the instrument includes scientists and students at Virginia Tech and the University of Texas at Dallas (UTD); the project is funded by NASA grant NNX12AF30G. The capacitance manometer is intended to be used on small satellites, such as CubeSats, which have a constrained power budget compared to large satellites.

There are two goals of the capacitance manometer project. The first is to expand the sensitivity of capacitance manometers into a much lower pressure range, in order to create a reliable pressure sensor for low earth orbit (LEO) missions. Commercially available capacitance manometers are able to measure to pressures of 10^{-5} Torr, however a pressure transducer capable of measuring pressures on the order of 10^{-8} Torr is necessary for low pressure environments such at the ionosphere and thermosphere. The second goal is to create a viable pressure transducer able to operate at a low power level. Currently Bayard-Alpert type ion gauges, utilizing a heated tungsten filament to ionize gases, are most commonly used as pressure instruments for LEO applications. These devices are unsuitable for continuous use on small satellites due to their large power requirements (Earle and Lee). The ideal capacitance manometer for LEO applications will be able to operate using orders of magnitude less power than a filament, while still providing accurate data measurements.

The capacitance manometer utilizes the physics of a capacitor to produce a changing capacitance that is related to a pressure differential. A capacitance manometer consists of one flexible membrane and one mesh grid. When a pressure differential acts on the flexible membrane it deflects, causing the separation between the two plates to change. The effect this has on capacitance can be seen in the equation below, where C is capacitance, ϵ_0 is the permittivity of a vacuum, ϵ_r is the permittivity of the dielectric material separating the plates (in this case 1), A is the surface area of the two plates, and d is the distance between the plates.

$$C = \epsilon_r \epsilon_0 \frac{A}{d} \tag{1.1}$$

Objectives:

1. Describe the vacuum chamber testing environment for the capacitance manometer.
2. Determine appropriate means of measuring the capacitance changes as a function of pressure.
3. Develop a test fixture to enable vacuum chamber testing.
4. Test the capacitance manometers using benchtop measurements and vacuum chamber measurements.
5. Perform capacitance and differential pressure measurements and present the results.
6. Characterize the capacitance vs. differential pressure relationship.
7. Determine viable directions for future development of the capacitance manometer.

The first two objectives are covered in Chapter 2, where the testing hardware, means of measurement, and developed test fixture are described. Objectives 3-6 are discussed in Chapter 3, where the testing procedure, results from preliminary testing, and characterization of the capacitance manometer are addressed and presented. The final chapter addresses objective 7, presents conclusions and suggests directions for future work.

1.1 Literature Review

The development of this low power, high sensitivity instrument is unique, as there is little previous work on this topic. However, the foundational concept of capacitance manometery is widely utilized in commercial vacuum systems. Figure 1.1 is from a sales catalog of a large vacuum system distributor (provide the reference - vendor name and catalog number) and shows the comparison of commercially available pressure instruments and their suitable pressure ranges.

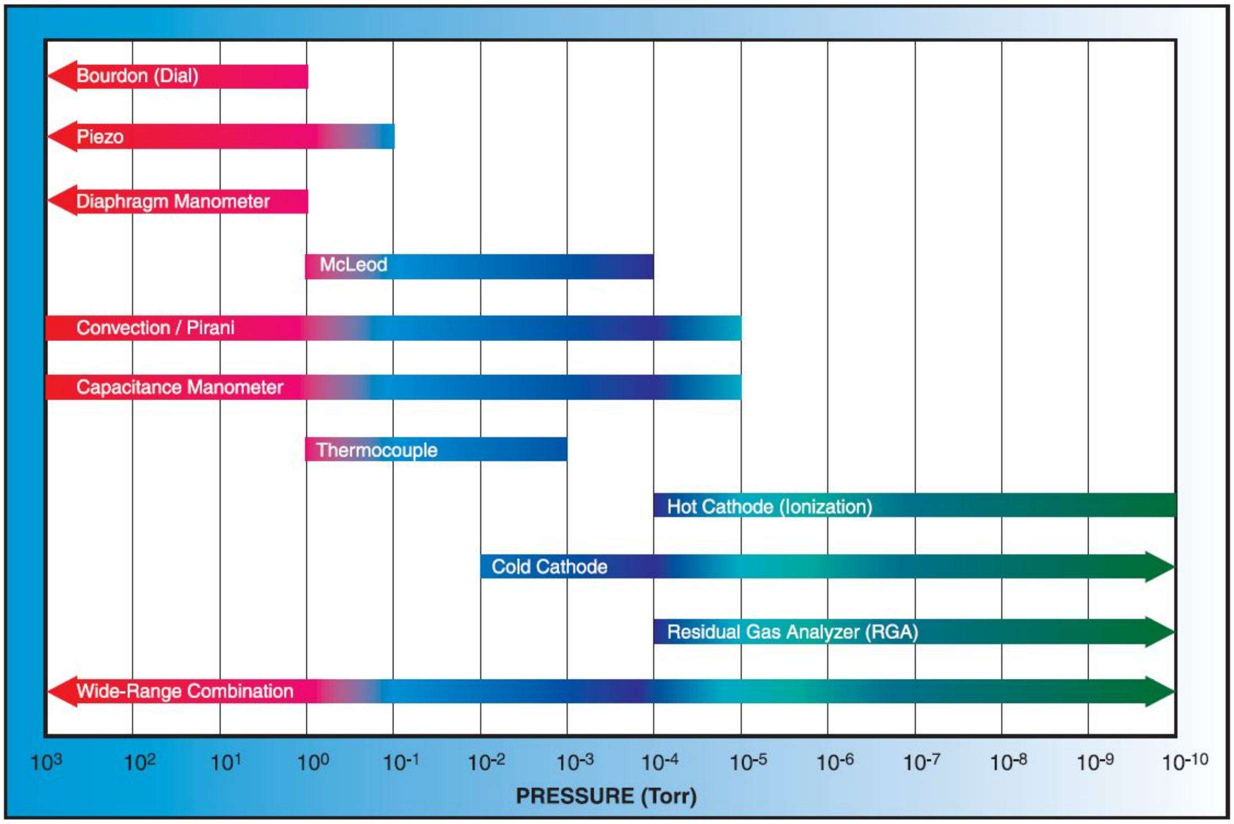

Figure 1.1: **Pressure Instrument Comparison.** Image from Lesker Sales Catalog showing suitable pressure ranges of commercially available pressure measuring devices for vacuum systems (Kurt J. Lesker Company).

As seen in Figure 1.1, commercially available capacitance manometers have a lower limit of 10^{-5} Torr. In the case of commercially available capacitance manometers, the thin flexible membrane is one side of a sealed diaphragm of a known pressure. The capacitance is measured between the membrane and fixed electrodes positioned a known distance from the membrane diaphragm. Figure 1.2 shows the construction of a typical, commercially available capacitance manometer.

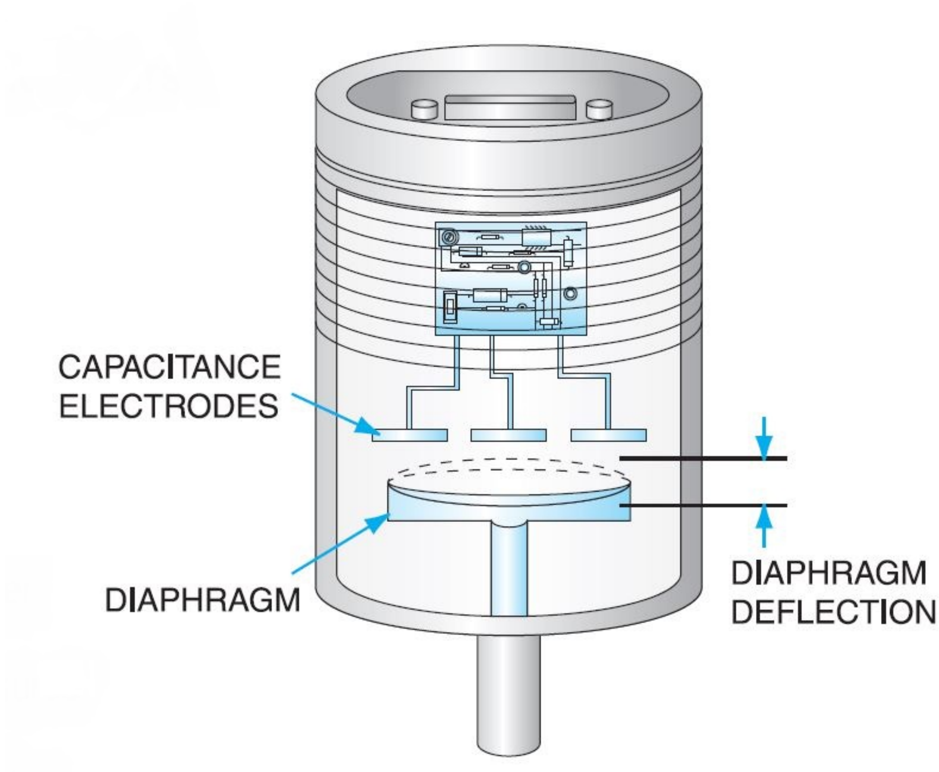

Figure 1.2: **Commercially available capacitance manometer.** Internal construction of a typical, commercially available capacitance manometer (Kurt J. Lesker Company).

Although these capacitance manometers are very accurate, they are not able to measure the low pressures typically present in the LEO environment. In attempting to extend this useful pressure range, a new capacitance manometer has been designed, fabricated, and tested by the UT Dallas and Virginia Tech teams.

Chapter 2

Test Procedure and Setup

2.1 Capacitance Manometers

The capacitance manometers developed for this project are microelectromechanical systems (MEMS) fabricated using micromachining technology by UTD. The capacitance manometer is constructed of a thin flexible membrane and a thicker, inflexible copper mesh grid. The flexible membrane on the capacitance manometers is gold plated polyimide with a diameter of 1 cm and a thickness of 1.4 μm. The airgap between the flexible membrane and the mesh grid is approximately 10 μm. As the differential pressure across the membrane changes the membrane deflects, resulting in a measurable capacitance change between the membrane and the grid.

The simulation software COMSOL was used by UTD to design the capacitance manometer. With simple structures the simulations are typically very accurate, however with more complicated designs of multiple layers (as was our device) the accuracy of the simulations becomes more difficult to verify (Lee, 2016). From simulation the manometers are designed to sense pressure differentials above 9x10^{-9} Torr; their capacitance measures 23.28 pF when experiencing no pressure differential. Simulation results also show a pressure differential of 7x10^{-6} Torr will result in capacitance change of 11 pF. Although the flexible membrane is delicate, it is expected to remain functional when experiencing pressure differentials as high as 1x10^{-2} Torr in a controlled environment. Several problems with the manometers arose during testing due to the delicate nature of the manometer, mainly related to the flexible membrane and the electrical connection pads. To mitigate these problems multiple iterations of the manometers were fabricated at UTD in response to feedback provided from testing conducted at VT. In total, three different versions of the manometer were fabricated. Other problems arose when integrating the manometer with the detection circuitry, as described in more detail below. The next few sections describe the testing process for each of the manometer versions, and describe changes made to mitigate issues observed during testing.

2.1.1 Manometer Version 1

The delivery of the first version of the capacitance manometer provided a tangible, testable product that met all initial design specifications, but which proved to be difficult to electrically connect to the measurement electronics. The solder pads provided with this version were very thin and were easily removed through gentle friction. The first attempt at soldering to these pads showed that gently placing the tip of the soldering iron onto the pads was enough to scrape away the conductive pad. Additional attempts at soldering showed another issue - the heat of the flowed solder would not stick to the manometer pad and appeared to burn through the pad. In order to provide a more uniform heat source, a heat gun was used to heat to the manometer structure after preparing the solder surface by applying solder paste to the pad. As in the earlier trials, the solder flowed but then pooled into a sphere and rolled off the solder pad. Subsequent visual inspection of the pad showed what appeared to be a spot on the solder pad where the solder had burned through the pad. In attempting to solve this problem, several alternative methods of connecting to the solder pads were attempted.

The manometers were tested using an LCR meter (Agilent E4980) to obtain as much information as possible about the connectivity problems. A tweezer probe was used to measure the capacitance of the initial static manometers. The thin solder pads proved problematic again as the slight friction of the tweezer probe was enough to scratch away the pads and prevent any capacitance measurements.

This version of the manometers maintained a small form factor of 2 cm x 2 cm, which created an additional problem related to placing the detection circuitry near the manometer. Close proximity of the detection circuitry is necessary to minimize capacitance from the connecting leads that could bias the measurements. This problem was eventually resolved through a separate breakout board, as discussed later.

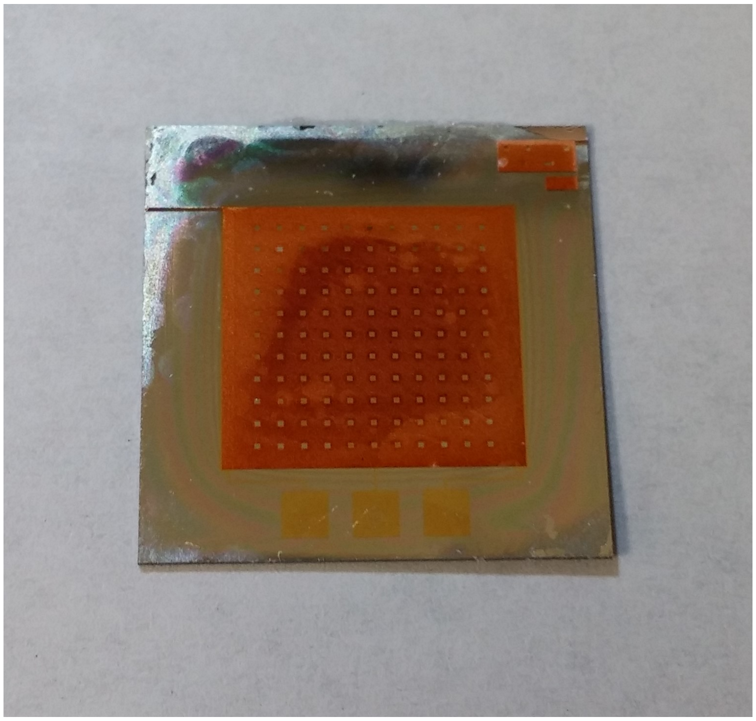

Figure 2.1: **Manometer Version 1.** Image showing the thick, inflexible copper mesh grid. The small gold solder pads are faintly visible on the bottom edge of the photograph.

2.1.2 Manometer Version 2

The second generation devices improved upon the initial design by thickening the solder pads (20-25 μm) to allow for easy connection, and by gold plating all copper surfaces to reduce oxidation. After testing various soldering methods, an acceptable solder joint was eventually achieved. The final method for soldering to the pads included using solder paste to allow for a consistent and controllable amount of solder, and using a sweeping motion of the iron across the pad to produce consistent heat transfer. Although the pads were thicker, the problem of heat transfer from the soldering iron to the pad remained. A plausible hypothesis for this behavior is that the manometer device itself is a large thermally conductive surface relative to the pad dimensions, which may cause heat to conduct through the chip rather than staying localized on the solder pad. In other words, the conductive capacitor plate may be acting as a heat sink for the solder pads. A careful sweeping motion across the pad allows the pad to heat more uniformly, allowing a successful solder joint to be achieved.

Thickening the solder pads introduced another problem inherent to the manometer chip and its construction. The solder pads exhibited a tendency to pull off the manometer chip when stress was applied to a connected wire. The force required to tear away a solder pad did not appear to be uniform, and may be an indication of non-uniformities in the fabrication process. Additionally the force needed to pull off a pad seemed to increase as the manometer chip cooled after a solder joint was created. This may indicate a lack of adhesion from the solder pad to the surrounding material that is worsened when thermal energy is introduced.

Manometer version 2 did not address the problem of keeping the detection circuitry in close proximity to the manometer chip. The small breakout PCB created for the version 1 devices was reused in this version to allow the detection circuitry to be located near the sensor.

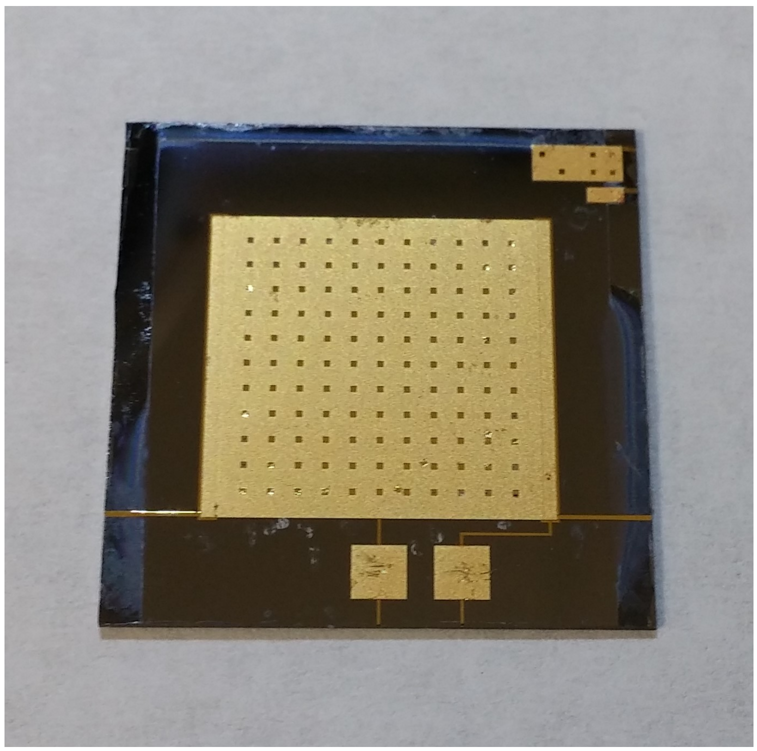

Figure 2.2: **Manometer Version 2.** Image showing the gold plated copper surfaces. The thicker inflexible mesh grid is shown with the thicker, gold plated solder pads visible along the bottom edge of the device.

2.1.3 Manometer Version 3

The third version of the manometer addressed the requirement of keeping the detection circuitry close to the sensor by increasing the size of the chip to accommodate the measurement electronics. This modification allowed the detection circuitry IC (integrated circuit) to be soldered onto the board very near the sensor, thereby minimizing the capacitive bias that could be introduced by long leads. The manometer aperture size remained the same as the previous two versions. The primary problem with this version was the size of the solder pads for the SMD (Surface-Mount Device) detection circuitry. The solder pads for the IC legs are very small. The solder problems from the previous version remained, and the previously developed technique for soldering to the device proved to be unsuitable. To mitigate this issue for testing, conductive silver epoxy was tried as a way to make electrical connections to the manometer chip, however the viscosity of the silver epoxy and the spacing of the ICs legs prevented it from being a viable solution. Multiple attempts were made to solder the IC to the manometer chip using various techniques, however none were successful. Due to the difficulty in connecting the detection circuitry to the manometer chip, manometer version 2 was determined to be the best design for functional testing.

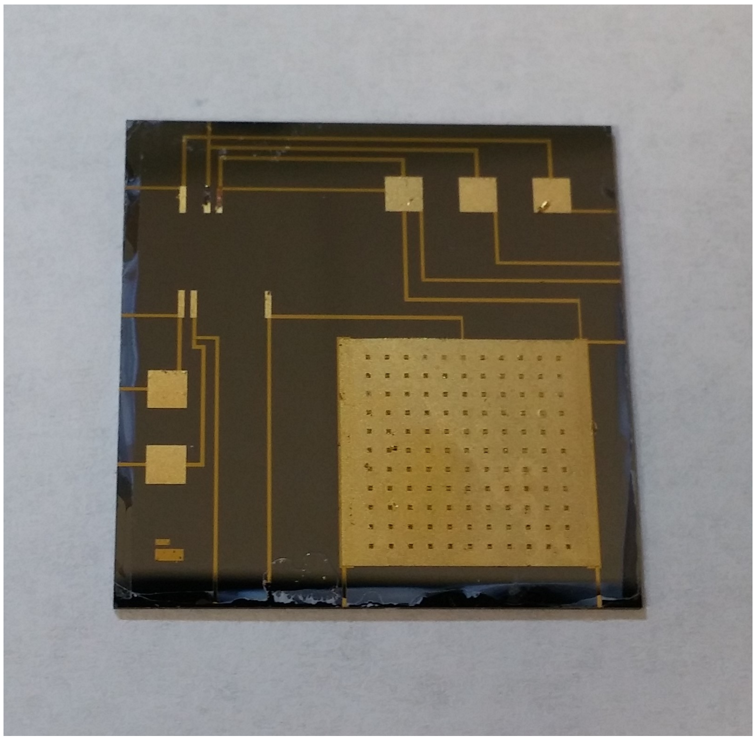

Figure 2.3: **Manometer Version 3.** The thicker inflexible membrane is located in the lower right sector of the device. The thin gold pads located in the upper left sector are designed for connecting the SMD measurement chip. Additional solder pads are included to provide appropriate I/O connectivity to the SMD measurement chip.

2.1.4 Measured Manometer Baseline Characteristics

The baseline capacitance of the manometers is initially measured using the Agilent E4980 LCR meter at standard room temperature and pressure, with no differential pressure across the membrane. Table 2.1 shows the data for the version 2 devices. All measurements are performed with the tweezer attachment, using an excitation voltage with a frequency of 100 kHz and an amplitude of 10 mV. The capacitance and resistance of the manometer chips are measured using the parallel and series equivalent circuit models, represented by a subscript p and s, respectively (need to explain the differences). Two manometers show values that may indicate functionality. They are denoted by superscripted asterisks after their identification numbers in Table 2.1.

Table 2.1: **Manometer benchtop measured values.**

ID Number	C_p	R_p	C_s	R_s
0814-6*	1.48 nF	1.747 kΩ	2.046 nF	477.6 Ω
0814-5	10.5 nF	3.47 Ω	19.7 μF	3.47 Ω
0813-2	8.9 nF	3.17 Ω	27.9 μF	3.16 Ω
0813-1	512 pF	112.9 Ω	388 nF	112.7 Ω
0813-6	-2.9 nF	2.158 Ω	-200 μF	2.16 Ω
0813-5	7.8 nF	2.96 Ω	35.7 μF	2.97 Ω
0814-9	-506 pF	12.54 Ω	-27.2 μF	13.52 Ω
081415-1	1.39 nF	2.47 Ω	294 μF	2.47 Ω
081415-2	2.84 nF	2.58 Ω	129 μF	2.57 Ω
0814-8*	536 pF	9.79 kΩ	586 pF	826 Ω

After using the baseline measurements to select the best candidate devices for further testing, we proceed to perform sensitivity tests in vacuum to quantify the performance of the manometers in the presence of changing pressures and temperatures.

2.2 Testing Environment

2.2.1 Vacuum Chamber

The vacuum chamber used for testing the manometers is an original design made specifically for the purpose of testing the capacitance manometers, seen in Figure 2.4. By including an automated nitrogen leak valve on one side of the quasi-symmetrical vacuum chamber, it is possible to test at desirable pressure differentials while maintaining a stable pressure environment. The vacuum chamber uses a roughing pump to create a weak vacuum in the system. A cryogenic pump is then used to reduce the vacuum level to the range of interest, in accordance with the design specification and simulation results from the CAD-assisted MEMS design. The cryogenic pump reaches a base pressure level of $7\text{x}10^{-8}$. A base pressure of $3\text{x}10^{-8}$ Torr can be achieved by heating the external walls of the vacuum chamber while the cryogenic pump is active.

The pressure chamber sections can be isolated from the medial equilibrium chamber using solenoid-controlled gate valves. Additionally, the medial equilibrium chamber can be isolated from the cryogenic pump by closing a manual gate valve. The two pressure chambers are isolated from each other through the manometer test fixture, which allows for a pressure differential to be applied to the capacitance manometer by adjusting the leak valve. A flexible bellows is used at the location the capacitance manometer test fixture to allow for easy installation of each test sample. Both left and right pressure chambers have dual feedthrough flanges to allow for flexibility in the mounting orientation of the test fixture. Each pressure chamber has an ion gauge (Lesker G100F) attached to allow for pressure measurements at low pressures. The ion gauges have an upper limit of 1x10^{-4} Torr, so a thermocouple (Lesker KJL-5311) is attached to the left pressure chamber to enable pressure measurements at levels that are higher than this upper limit. The ion gauges and the thermocouple are controlled by the Agilent XGS-600 Gauge Controller. The XGS-600 is interfaced with a computer through serial connection, allowing all three pressure readings to be recorded during testing. A LabVIEW GUI is used to record and plot this information in real time.

The nitrogen leak valve is controlled by a LabVIEW GUI to raise the pressure in the left pressure chamber. This increase in pressure creates the pressure differential that changes the capacitance of the device under test, as described earlier. Because the left pressure chamber is able to be isolated from the cryogenic pump via a solenoid valve, pressures as high as one atmosphere (760 Torr) can be realized and measured, while simultaneously maintaining a low pressure vacuum in the right pressure chamber. The pressure is only able to be increased in the side of the chamber that houses the leak valve (in this arrangement, the left pressure chamber), however, the feedthroughs on both pressure chambers allow the manometer to be oriented with either the grid of the membrane on the side housing the leak valve. Consequently the differential pressure created can either increase or decrease the distance between the capacitor plates when experiencing a differential pressure, depending on the mounting. This flexibility allows for testing the full functionality of the capacitance manometer.

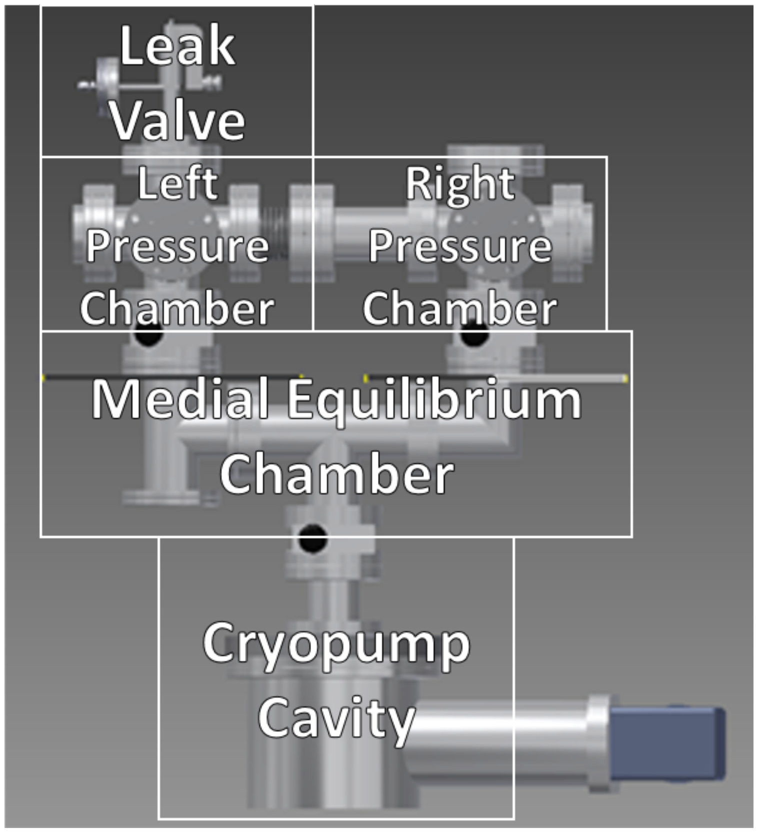

Figure 2.4: **CGI image of vacuum chamber.** The capacitance manometer is installed at the intersection of the left pressure chamber and the right pressure chamber. Nitrogen is leaked into the system via microcontrolled leak valve attached to the left pressure chamber. Both pressure chambers feed into the medial equilibrium chamber via solenoid valves. The medial equilibrium chamber connects to the cryopump cavity via manual gate valve. Crump, D. (2013). *Capacitor Manometer Differential Pressure Test Chamber User Manual.* M.Eng. Project and Report, Virginia Tech. Used under fair use, 2016.

2.2.2 AD7747 Chip

The Analog Devices AD7747 chip is used as the detection circuitry for the capacitance manometer transducer. The AD7747 is a 24 bit $\Sigma - \Delta$ capacitance-to-digital converter (CDC) with high accuracy (10 fF) and an input range of 8 pF. It has an on-chip programmable digital-to-capacitance converter which allows the chip to accept a common-mode capacitance up to 17 pF. This allows for an effective measurement range of 0-25 pF. The chip has a 2-wire, I^2C-compatible serial interface for data transfer and communication. The AD7747 also features an on-chip temperature sensor.

The AD7747 is used for this project because of its high accuracy and its capacitance input range, both of which are well suited to the capacitance manometers being tested. Given the characteristics of the manometer, the chip boasts several advantages for testing. First is its high accuracy within the capacitance range of the manometer. The CDC chip has an accuracy of 10 fF which allows for high-resolution data measurements of the capacitance manometer and enables very small capacitance changes to be measured. A second benefit of the AD7747 chip is its ability to output a digital signal via an on-chip serial interface. This is useful as it allows for a wide margin of compatibility with other systems. Additionally, the digital output is more noise tolerant than an analog signal and is less affected by parasitic effects introduced in the cabling and connectors that are necessary to interface with the computer-based data acquisition system.

The evaluation board associated with the AD7747 chip is used to provide an interface with a computer for controlling the chip and acquiring data from the version 2 manometers. The board uses a 10-pin male header connection that enables external AD7747 measurement chips to connect to the board and utilize its on-board power supply and I^2C interface. Because of this, a measurement chip can be placed in close proximity to the capacitance manometer inside the vacuum chamber. The evaluation board also has a USB driver that enables USB connectivity to a computer for easy integration and connectivity.

2.2.3 Manometer Fixture

A unique test fixture comprised of several components is needed to integrate the capacitance manometer into the vacuum chamber. To support the AD7747 measurement chip being placed in close proximity to the capacitance manometer, a small break-out PCB is used to mount the AD7747 chip, as seen in Figure 2.5. The board has the AD7747 chip mounted in the middle with through-hole solder pads on the exterior edges. To overcome solderability issues presented by the manometers, two test fixtures utilizing different forms of electrical connection, have been created to accommodate the capacitance manometer and the AD7747 chip.

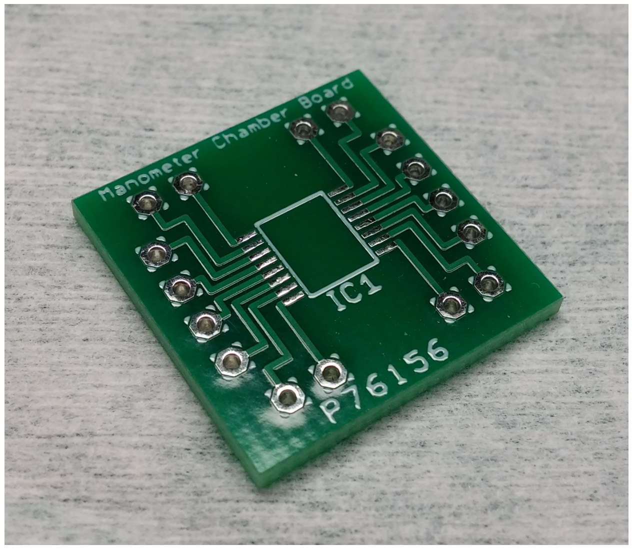

Figure 2.5: **Image of break out board for AD7747.** The AD7747 chip is soldered to the center of the break out board. The board allows easy connection to the chip via through hole pads.

Figure 2.6 shows a manometer fixture that utilizes the break out-PCB but uses conductive silver epoxy to make the electrical connections. The break out PCB and the capacitance manometer are mounted using vacuum epoxy onto a piece of glass that measures 40 mm x 50 mm. The glass slide has a circular cut-out slightly larger than the manometer membrane to accommodate the capacitance manometer aperture. The glass is used to provide a non-conductive mounting material for the exposed interconnect wires that protrude through the break out PCB. The glass slide is then mounted onto a copper gasket that has a rectangular cut-out. The gasket is machined to have a slightly smaller inset dimension to allow the manometer to be epoxied to the gasket, creating a complete seal around the edges of the glass slide.

Vacuum safe silver epoxy is used to make the electrical connection to the capacitance manometer due to the delicate nature of the connecting pads. Two 30 AWG stranded wires from the break out board are used to connect the capacitance manometer to the measurement chip. These wires are made as short as possible to reduce the risk of introducing any parasitics between the capacitance manometer and the measurement chip. Wires are soldered to the measurement chip break out board with female D-sub connector pins attached to each wire. This facilitates quick connection to the manometer test fixture. The fully assembled fixture can be seen in the figure below.

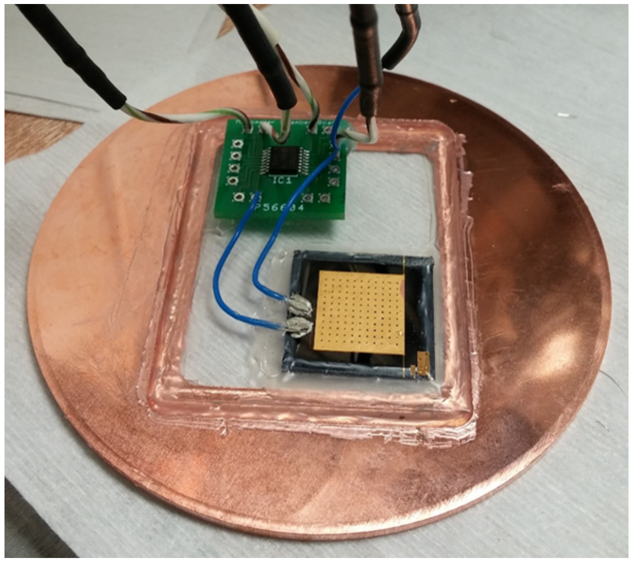

Figure 2.6: **Capacitance manometer test fixture.** The assembled test fixture ready for mounting in the vacuum chamber. The glass slide is epoxied onto the copper gasket using vacuum epoxy. The manometer is vacuum epoxied around the edges of the chip to maintain a vacuum seal. Two wires are silver epoxied to the connection pads on the manometer and are soldered to the break-out PCB housing the AD7747 measurement chip. The break-out PCB is vacuum epoxied to the glass. Short wires with female D-sub connector pins are soldered to the appropriate I/O connections of the AD7747 chip.

This fixture is ideal for testing because of its low profile and ease of installation into the vacuum chamber. The offsetting disadvantage of this fixture is the time needed to prepare a sample for installation, but this can be partially mitigated through efficient planning and parallel task management. Multiple components are epoxied at different stages and need to fully cure between steps to ensure that the manometer remains intact and functional. The fixture becomes unusable if it is damaged at any point during the assembly, so careful handling is required at all stages of assembly.

2.2.4 Vacuum Chamber Connection

Inside the vacuum chamber, a vacuum safe D-sub connector is used to connect to the internal side of the vacuum feedthrough. Wires are then run to the manometer test fixture where male D-sub pins are attached to each wire. This allows for quick connection to the manometer test fixture, which reduces vacuum pump-down time during the iterative testing process. To prevent the D-sub pins from shorting to each other or to the walls of the vacuum chamber, shrink tubing is applied around each connection point. In total there are 5 connections between the break out board and feed-through on the vacuum chamber.

On the exterior of the vacuum chamber, a D-sub connector is used to interface between the vacuum chamber feedthrough to the measurement chip evaluation board. The wires from the D-sub connector are attached 10 pin female header assembly that plugs directly into the evaluation board. The evaluation board then connects to a computer for data capture via USB connection.

2.3 Noise/Problem Sources

2.3.1 Membrane Distortions

The flexible membrane tends to deform slightly due to the measurement technique the detection circuit uses. The AD7747 measurement chip applies an excitation voltage to measure the capacitance of the manometer. Additionally, the chip applies a DC voltage as a bias for the AC excitation voltage to ensure the excitation voltage does not clip. In our test setup, the AD7747 chip is operated at VDD = 3.3 VDC. Via the measurement chip GUI, the excitation voltage level is manually set to be VDD/8, giving an excitation voltage of 412.5 mVpk. The DC bias voltage is fixed at VDD/2 giving a DC bias of 1.65 V. When a capacitance manometer is measured via the AD7747 chip, the manometer therefore has a maximum voltage of 2.0625 V applied. This voltage creates an electrostatic force between the two plates, causing the flexible membrane to be attracted to the mesh grid. Multiple samples showed that this force between the plates was enough to cause the plates to become shorted and unusable. Figures 8 and 9 below show photos of the flexible membrane of a manometer before and after installation and testing in the vacuum chamber. Note that when the manometer was removed it registered as a short as measured by the AD7747 chip.

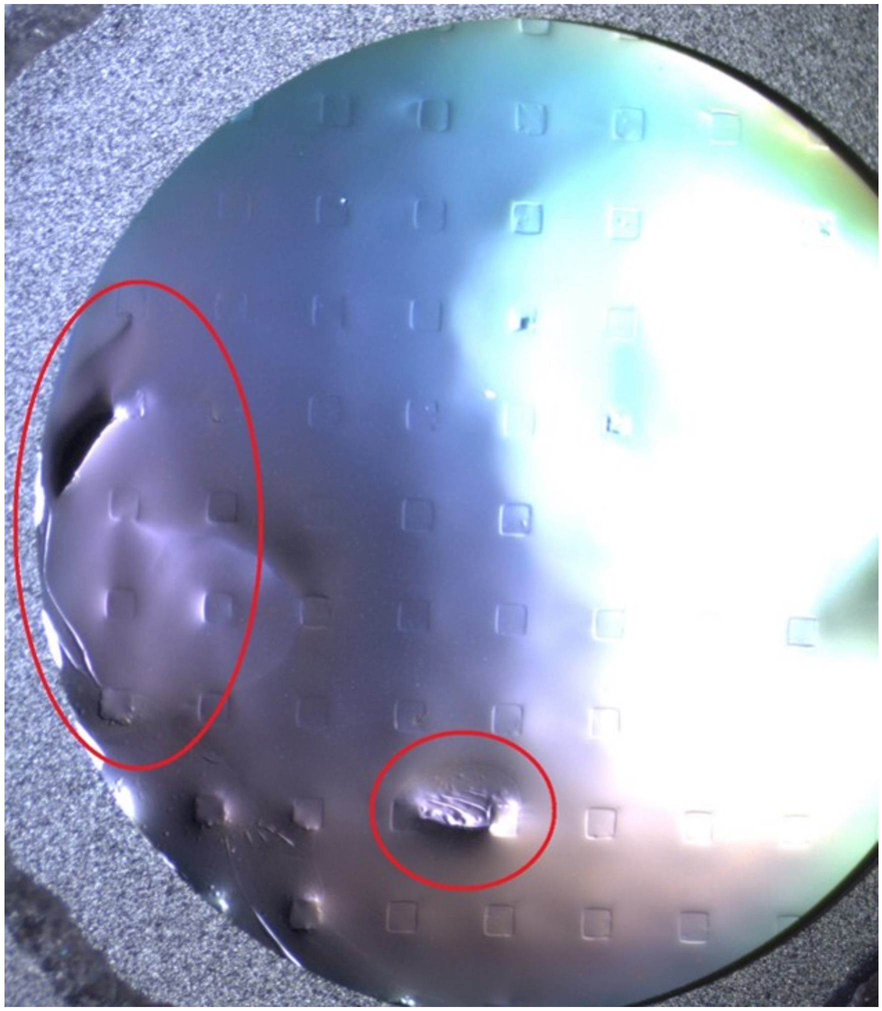

Figure 2.7: **Close-up photo of the manometer membrane before testing in vacuum.** Circled areas are regions that were damaged during fabrication or shipping.

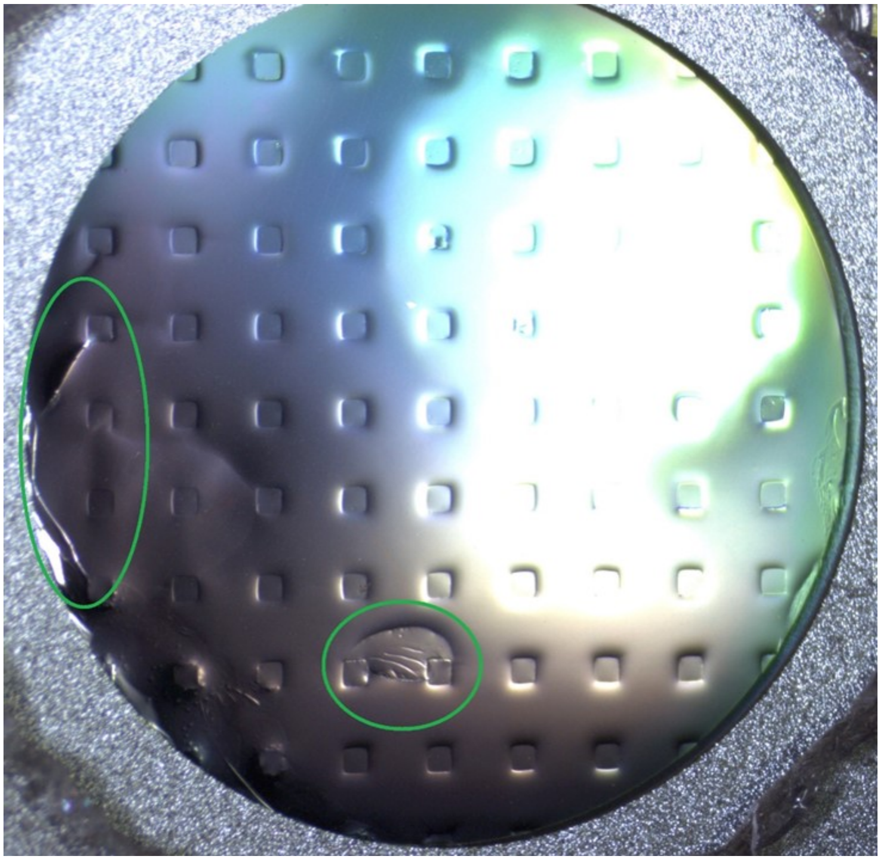

Figure 2.8: **Image of same manometer shown in Figure 2.7 after testing in vacuum.** The circled areas are noticeably different than the previous figure. Also note the enhanced dimple pattern.

In Figure 2.7 the manometer has appreciable deformations, as indicated by the red circles. It also has a very light dimple pattern that coincides with the structure of the grid electrode. This dimple pattern correlates very well with the square holes in the mesh grid, and it appears on all the manometer samples. After consulting with our UTD colleagues, it was concluded that the pattern is a result of the etching process, but the device is deemed suitable for use. The large deformations in the images are not standard, and our hypothesis is that these features were formed during handling or shipping of the manometers at some point between fabrication and assembly of the manometer test fixture. The large deformations provide an additional dimension of non-uniformity to the flexible membranes for comparison with the after image.

Figure 2.8 shows the membrane after the measurement chip voltage was applied in the vacuum chamber. The light dimple pattern present in the before image appears to have been enhanced to a more distinct dimpled pattern. The two deformations indicated in Figure 2.7 by the red circles appear to have flattened, as is noted by the green circles in Figure 2.8. Of special note is the deformation in the bottom of the flexible membrane, which appears to have been completely flattened to the point of extending towards the mesh grid, as opposed to away from the mesh grid in the before image.

The effects of the electrostatic force caused by the measurement chip are clear, but the reasons for the prominence of the dimpled pattern in the after image is not clear. One hypothesis is that the flexible membrane is being attracted to the mesh plate with enough force to actually push through the square holes of the mesh grid, permanently enhancing the dimples. The flattening of the deformation in the bottom of the flexible membrane adds credibility to this theory. The electrostatic force would cause the membrane to pull towards the mesh grid, flattening any deformation protruding away from the mesh grid if said deformation is located where the grid is solid. The deformation is located between four of the mesh grid holes, and, as mentioned previously, has been flattened to the point of protruding toward the mesh grid. Figure 2.9 shows a closer image of the deformation after applying the measurement chip voltage.

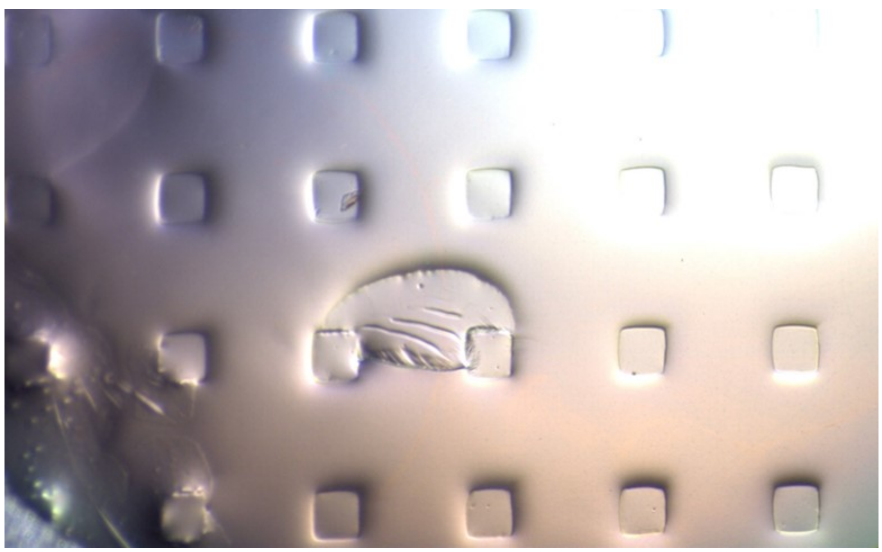

Figure 2.9: **Close up of the membrane deformation.** Close up of membrane deformations seen in Figure 2.8.

2.3.2 Test Setup

Care has been taken to reduce the amount of noise and interference injected into the system, however there are still several points in the manometer connection that could be possible sources of noise or error. Starting from the capacitance manometer chip, the use of silver epoxy to connect to the chip provides a safe and reliable means of electrical connection, but the mixing ratio of the 2-part epoxy influences its conductivity. In early manometer fixtures there were cases of the epoxy not being conductive enough, causing certain manometer fixtures to be deemed unusable.

Another potential point of noise is the 30 AWG hook-up wire used to connect the manometer to the AD7747 breakout board. Although the manometer fixture is seated inside of a grounded vacuum chamber, creating a Faraday cage, inside the chamber the manometer is in close proximity to the measurement chip. The measurement chip has regulated DC power and ground signals, as well as three digital lines. Despite the low power levels of the signals on the digital lines, they carry square wave signals that have high frequency components which could be a source of EMI on the hook-up wires. Although any noise injected into the system from an induced current would be small, the observed capacitance changes are on the fF scale; therefore, small magnitudes of noise caused by the induced currents in the hook-up wires could be substantial.

The next component in the signal flow is the AD7747 chip. The chip has inherent noise within the capacitance measurement, however this is very small. A conversion rate of 4.1 Hz is used for data collection and this correlates to a noise level of approximately 5.5 aF (or 5.5 x 10^{-6} pF). Due to the high bit resolution of the chip, the output value tends to have a non-periodic oscillation centered around the actual capacitance value of the device being measured. When bench testing with fixed capacitance values this oscillatory behavior is negligible, indicating that the non-periodic oscillatory noise seen in the data is likely from parasitics in the test fixture.

The outputs of the capacitance measurement chip are all digital signals. The path from output of the chip to the input of the AD7747 evaluation board passes through several D-sub connectors as well as the feedthrough flange on the vacuum chamber. Any noise introduced into the system at this stage can be largely ignored due to the noise tolerance properties of digital signals.

2.3.3 Connectivity Concerns

One potential concern with the capacitance manometer is the quality of the electrical connection between the gold plated solder pad and the connecting wire using silver epoxy. The gold plating is relatively thick (approximately 1.2 μm) and there is potential for outgassing at the junction between the gold plating and silver epoxy. Au finishes tend to be more susceptible to contaminants during the fabrication process that are then volatilized and released when placed in a low pressure environment. This creates small voids in the interface of the Au plating and silver epoxy which could degrade the electrical connection between the two (Bulwith).

In the case of the manometer being tested, no special care was taken to remove contaminants from the surface of the solder pads. Additionally the manometer used for testing had not been soldered to or had any other mechanical forces or strain placed upon the solder pads prior to being installed in the test fixture and having silver epoxy used to connect the solder pad to the hook up wires.

Chapter 3

Results and Discussion

3.1 Preliminary Testing

Initial testing of the capacitance manometers confirmed the hypothesis that several of the manometers were not functional. In total, eight capacitance manometers were placed in the vacuum chamber for testing, and only one manometer showed a capacitance (the possible reasons for this will be explored and explained in the next chapter). The results below are all taken from the functioning sample. Multiple trials of each test were performed to characterize the data and to minimize any error.

3.2 Capacitance vs. Temperature Characterization (First Iteration)

The capacitance of the manometers exhibits changes as a function of temperature. This characteristic was discovered empirically, and the cause was found to be the filament-based ion gauges used to measure the pressure inside the vacuum chamber. The gauges rely on thermionic emission of energetic electrons, so it is unavoidable that this heat source affects the vacuum chamber walls and any structure mounted inside. This heat source affects the validity of measurements of the capacitance change caused by pressure differentials, and is the first parameter of the capacitance manometer that must be characterized. Using the AD7747 internal temperature sensor, initial tests show the temperature change caused by the ion gauges during testing is approximately 2° C above the starting temperature. The AD7747 chip is located in close proximity to the capacitance manometer and therefore provides a reasonable estimate of the temperature of the capacitance manometer during testing.

Initial testing shows the time to reach a steady state temperature to be approximately 30 minutes. To capture this information, the capacitance manometer is tested under no pressure differential to allow all capacitance changes to be directly related to the heating effects of the ion gauges. A single test, referenced in what follows as a sweep, is comprised of three parts: an initial static measurement time with ion gauges off to determine the baseline capacitance, a heating time where the ion gauges are turned on simultaneously, and a cooling time where the ion gauges are turned off simultaneously. The heating and cooling times are approximately 30 minutes to allow for the temperature plateau to be reached. Data from five sweeps are used to obtain a measurement of the expected capacitance change caused by the gauge-induced temperature change. In addition to empirical evidence provide by the sweeps, simulations are also performed to estimate the expected capacitance change relative to the actual temperature measurements of the AD7747 chip.

3.2.1 Filtered Capacitance and Temperature Data (First Iteration)

Five temperature sweeps are performed to capture the relationship between the capacitance manometer temperature and the manometers capacitance change. The temperature data are very noisy with outliers, therefore a median fit algorithm is used on both the capacitance data and the temperature data to minimize presence of outliers (the median fit algorithm used is included in Appendix A).

Another issue that is presented in the data is the bit resolution of the temperature data. The AD7747 chips primary use is for capturing capacitance data, and a lower bit depth is used for the temperature measurements. The chip only has a bit resolution of 0.1° C, so for the small temperature variations created by the ion gauges bit-level fluctuations are evident in the temperature data. Although the general shape of the curve is apparent, this causes problems when comparing the temperature data to the capacitance data. The data are passed through an eight point moving average filter 10 times to clean up the signal while maintaining the shape of the trends in the data.

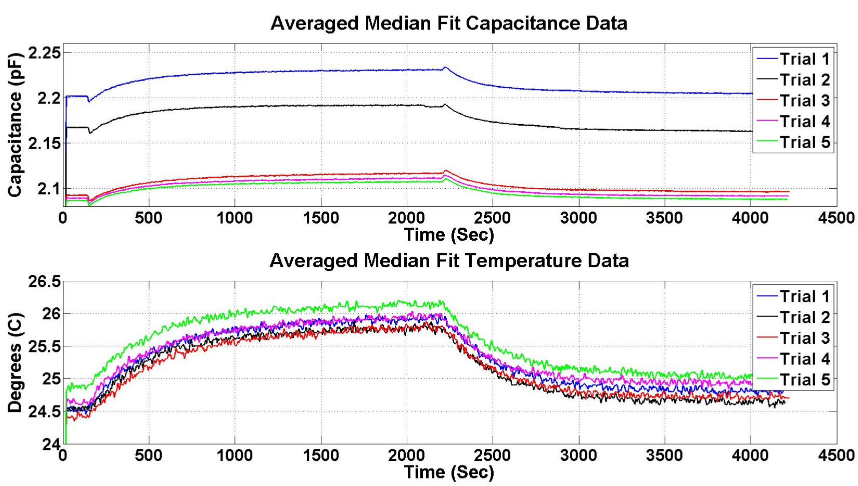

Figure 3.1: **Averaged and median fit temperature data (first iteration).** Median fit data passed through an averaging filter to minimize bit resolution distortion in the temperature data.

Simple visual analysis of Figure 3.1 shows that the baseline capacitance of the manometers changes between sweeps. The five sweeps were taken over the span of two days with ample time between sweeps for the ambient temperature inside the chamber to equalize with the ambient temperature of the room. The cryopump was constantly active over these two days, and also during the sweeps. The pressure of the chamber read by the ion gauges at turn off (at time 2200 sec) is noted in the Table 3.1.

Table 3.1: **Measured pressure of vacuum chamber at turn off of ion gauges.**

Trial	**Left Ion Gauge**	**Right Ion Gauge**
1	9.4E-7 Torr	1.5E-6 Torr
2	3.8E-7 Torr	5.5E-7 Torr
3	2.5E-7 Torr	3.6E-7 Torr
4	2.4E-7 Torr	3.3E-7 Torr
5	2.3E-7 Torr	3.2E-7 Torr

One possible explanation for the baseline capacitance decreasing over consecutive sweeps is that the differential pressure across the manometer is slightly increasing over time, allowing the manometer to read closer to its true static capacitance. Although this may seem logical, the data presented in the pressure differential section contradicts this hypothesis. Another possible reason the baseline capacitance is decreasing over time could be related to outgassing in the chamber. When powered on the ion gauges warm the interior of the chamber, causing some outgassing to occur. The consistently decreasing pressures seen in the table above are evidence of this. Additionally, there is a minimum pressure attainable inside the vacuum chamber, which is determined by a balance between the pump speed and the various leak rates of the flanges and outgassing of the surfaces. The manometer is handled carefully during the assembly of the test fixture to ensure it remains as clean as possible, however the manometer still has impurities on it from the fabrication process (as noted earlier, there could be contaminants on the Au plated surfaces of the manometer that are outgassing over time which would support this theory). Therefore it is also possible that while the ion gauges are on the manometer and test fixture are outgassing, reducing the level of impurities and giving a more accurate reading of the static capacitance.

The bit resolution noise in the temperature data is minimized by averaging, with the sharp peaks and valleys of the capacitance data largely unaffected. One negative effect of passing the data through a moving average filter multiple times is the loss of data at the beginning of the set. However, the data sets include a long static time at the beginning that is sufficient to allow a viable static capacitance and temperature to be calculated.

3.2.2 Normalized Capacitance and Temperature Data (First Iteration)

Using these static values, the capacitance and temperature data can be normalized allowing for better comparison of each temperature sweep. Figure 3.2 shows the normalized data set of the averaged, median-fit, filtered capacitance and temperature values.

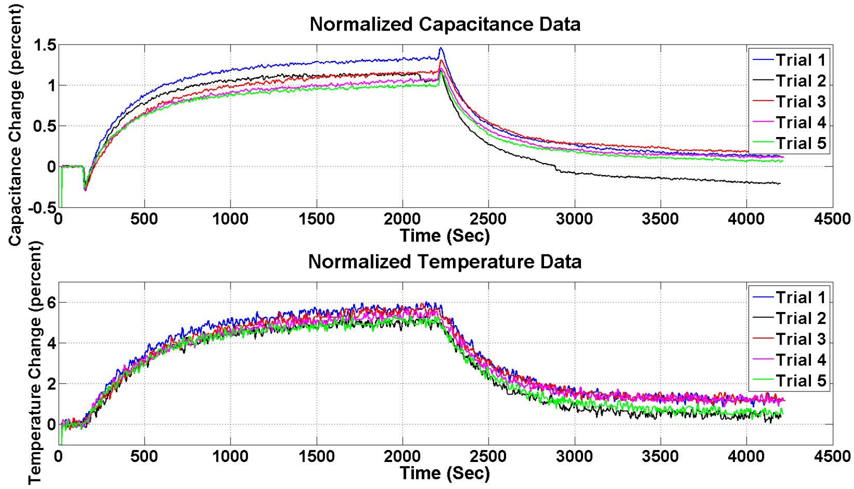

Figure 3.2: **Normalized temperature data (first iteration).** Normalized data for comparison of individual temperature sweep datasets.

The normalized data show some differences between each of the sweeps. All sweeps share the same normalized magnitude in the initial dip of the capacitance seen when the ion gauges turn on, however the temperature increase is not consistent among all five sweeps, causing the capacitance change to be inconsistent as well. A good representation of this is in comparing the first sweep, represented by the black line, and the fifth sweep, represented by the green line. In the temperature data, the first sweep is consistently warmer than the fifth sweep. This translates to the percent capacitance change also consistently being higher in the first sweep compared to the fifth sweep. Strangely, these results are more clear as the manometer is heating, and become less clear while the manometer is cooling (this behavior presents itself again in the simulations). The two plots show a logarithmic increasing relationship in the portion of the data corresponding to the ion gauges being on, and an exponential decay relationship in the portion of the data corresponding to the ion gauges being turned off. Despite the plots showing a large change, the capacitance change is only between 1 and 1.5 percent of the static capacitance value when the temperature change is between 5 and 6 percent of the static temperature value. The accuracy of the AD7747 chip allows the conclusion that these changes, though small, can be trusted.

3.2.3 Normalized Capacitance vs. Temperature Data (First Iteration)

The most telling plots to determine the relationship between the capacitance change and temperature change are shown in Figures 3.3 and 3.4, which show the normalized capacitance change vs. normalized temperature change for both the heating and cooling cycles. Second order polynomial best fit lines are included for comparison.

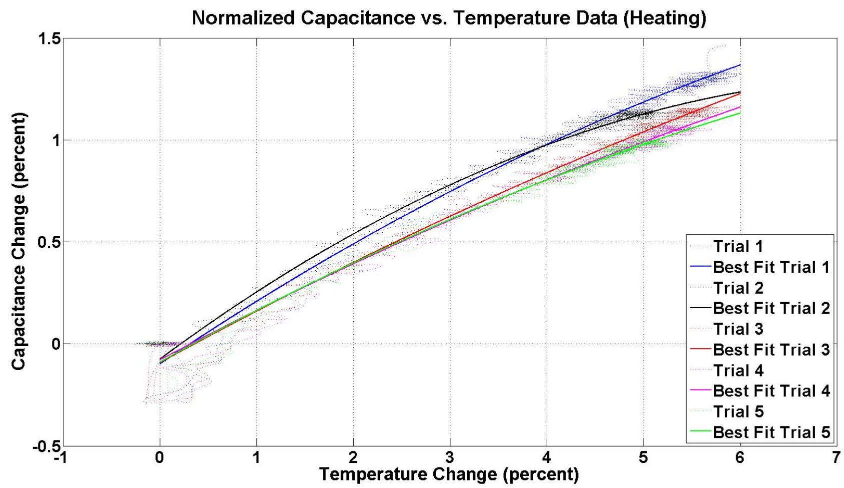

Figure 3.3: **Normalized capacitance vs. normalized temperature (first iteration, heating).** Normalized data for the heating cycles with ion gauges turned on. Best fit lines added for comparison.

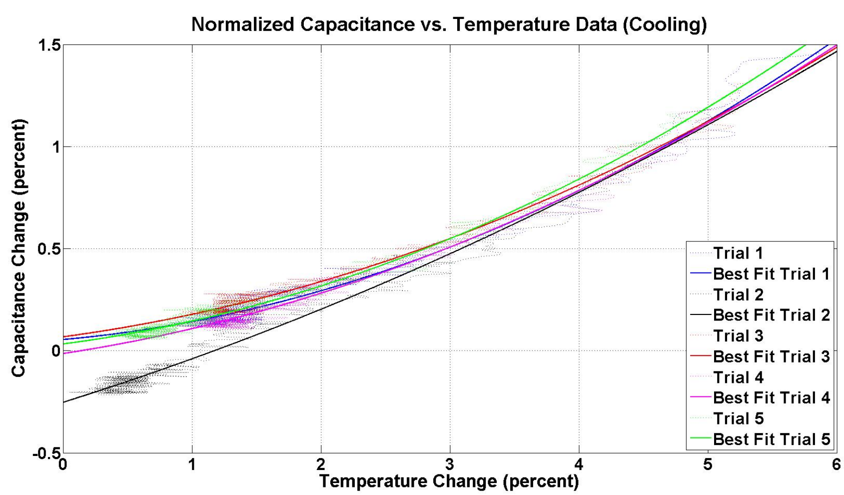

Figure 3.4: **Normalized capacitance vs. normalized temperature (first iteration, cooling).** Normalized data for the cooling cycles with the ion gauges turned off. Best fit lines added for comparison.

The plots above show a near linear correlation between the capacitance change and the temperature change, both in the heating and cooling portions. However, the two plots do not share the same magnitude for a given percent temperature change. One possible explanation is that the AD7747 chip is not heating or cooling at the same rate as the manometer chip. This is plausible since the manometer surfaces do not have the same conductive path to the circuit board and vacuum chamber.

Despite the magnitude differences the trials all have a similar slope, especially during the cooling cycles. Tables 3.2 and 3.3 give the coefficients of the best fit lines for the following second order polynomial equation.

$$f(x) = p1 * x^2 + p2 * x + p3 \tag{3.1}$$

Table 3.2: **Normalized capacitance vs. normalized temperature best fit coefficients (first iteration, heating).**

Trial	p1	p2	p3
1	-0.01242	0.3189	-0.09879
2	-0.02215	0.3512	-0.07545
3	-0.006467	0.2586	-0.09215
4	-0.007188	0.2497	-0.07864
5	-0.009893	0.2628	-0.08943

Table 3.3: **Normalized capacitance vs. normalized temperature best fit coefficients (first iteration, cooling).**

Trial	p1	p2	p3
1	0.03148	0.0565	0.05444
2	0.01461	0.1987	-0.2528
3	0.02522	0.08492	0.06782
4	0.02601	0.09579	-0.01407
5	0.02988	0.0823	0.03286

An anomaly in the heating data that is also present in Figure 3.2 is the magnitude differences between the two linear clusters of data in the heating portion of the sweep. As was seen earlier, the data from the first two sweeps (shown in blue and black above in Figure 3.1) are of a larger magnitude than the other three sets of data. Previously, the baseline capacitance was decreasing with each iteration, causing a large magnitude difference in the first two sweeps of data. This magnitude difference is unexpected in these plots because the data have been normalized to provide a more precise comparison.

The only notable change between test sweeps is the decreasing pressure in the vacuum chamber. This may point to convective heating inside the chamber as the cause of the changes observed. Simply, the gas surrounding the manometer is being heated and causing the fluid characteristics to change. As the fluid around the manometer changes, the thermal effects on the flexible membrane may allow it to move more freely. This may be considered unlikely due to the very low pressure present in the vacuum chamber, but consider that the difference in magnitude shown in Figure 3.3 is only 0.13%. Although visible given the scale of the plot, this is a difference that would be difficult to determine in a testing environment where the temperature change is 20° C, rather than 2° C. This small effect allows the anomaly to be noted, but ultimately, no strong conclusion can be made as to the source and how it would affect larger temperature ranges.

3.2.4 Anomalies in Data (First Iteration)

The primary anomaly presented in the dataset is presence of valleys and peaks in the capacitance data when the ion gauges are turned on and off, respectively. There are several possible causes of this anomaly. One hypothesis is poor voltage regulation to the testing system. All devices used during testing (this includes the cryopump, computer for capturing data, and the ion gauge controller) are connected to the same power source. When the ion gauges are turned on/off there could be a slight drop in wall voltage causing a transient in the system. This theory is unlikely though because the power draw from the ion gauge controller is insignificant in comparison to the power draw of the cryopump and computer.

Another theory is that the particles emitted, as well those ionized, by the filament wire are somehow causing these transients to appear. This theory is more likely when the geometry of the manometer, the location of the ion gauges, and the direction of the transient are all considered. The manometer is comprised of one mesh grid and one flexible, solid grid. The ion gauges are at the ends of the vacuum chamber such that when the filaments are heated, particles are emitted and ionized within tubular regions leading to each side of the manometer. The mesh grid effectively acts as a shield for the flexible membrane on the mesh grid side of the manometer, whereas the solid membrane side experiences all particle effects the ion gauges are causing. From Figure 3.2 the transient seen when the ion gauges turn on is a dip in the capacitance value, corresponding to the plate distance increasing, with a peak in the capacitance value when turned off, corresponding to the plate distance decreasing. If there were particle collisions on the flexible membrane from particles emitted by the ion gauge, and accounting for the shielding effect of the mesh grid, it would be logical that the plate distance should decrease when the ion gauges are turned on, causing a peak rather than a valley. The hypothesis of particle collisions pushing the membrane towards the mesh grid is proven false, however the ion gauges are still suspected of causing the transients. This idea can be tested by changing the location of the ion gauges so they no longer radiate axially towards the manometer. These data are presented in section 3.3.

3.2.5 Simulated Capacitance and Temperature Data (First Iteration)

Thermal modeling of the test system was performed by an undergraduate collaborator to validate the capacitance changes seen by the manometer when undergoing a temperature change. The actual temperature change measured by the AD7747 chip is used to seed the model, and the model uses nominal thermal characteristics of the materials used in the fabrication of the capacitance manometers. The results of the simulations are shown in Figures 3.5 - 3.9. Each plot corresponds to a single sweep, with the empirical capacitance and temperature plotted along with the modeled capacitance.

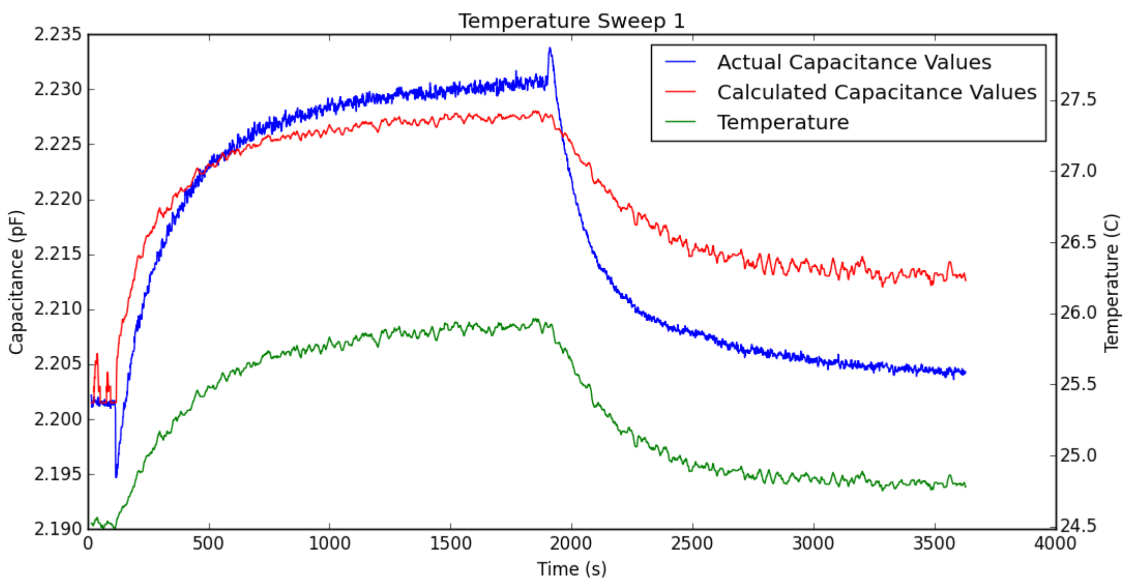

Figure 3.5: **Modeled capacitance change for trial 1.** Collected capacitance and temperature data plotted with modeled data for sweep 1. Figure generated by Matthew Francom.

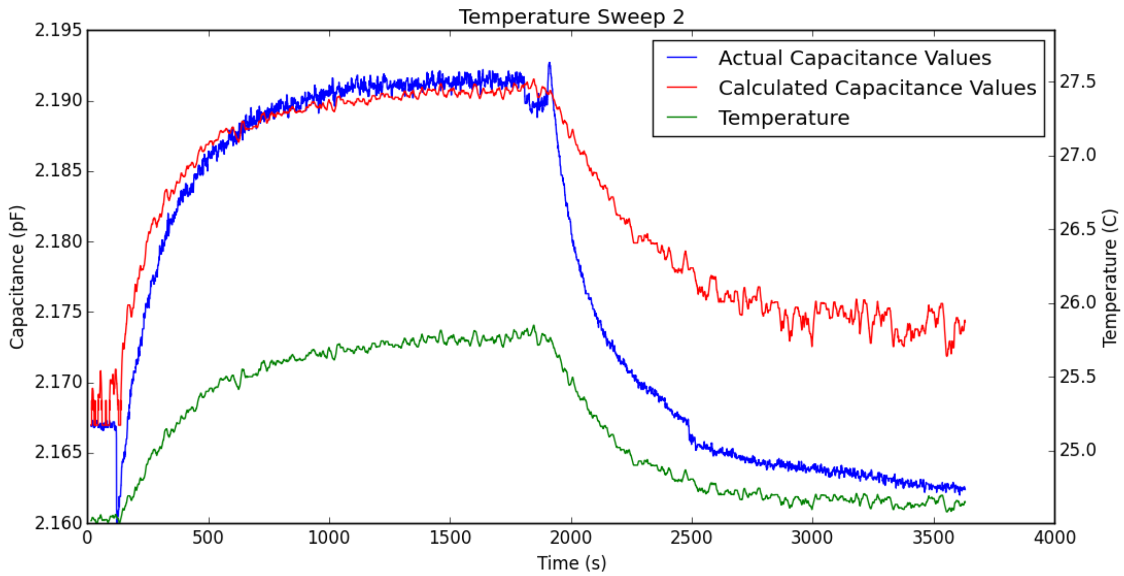

Figure 3.6: **Modeled capacitance change for trial 2.** Collected capacitance and temperature data plotted with modeled data for sweep 2. Figure generated by Matthew Francom.

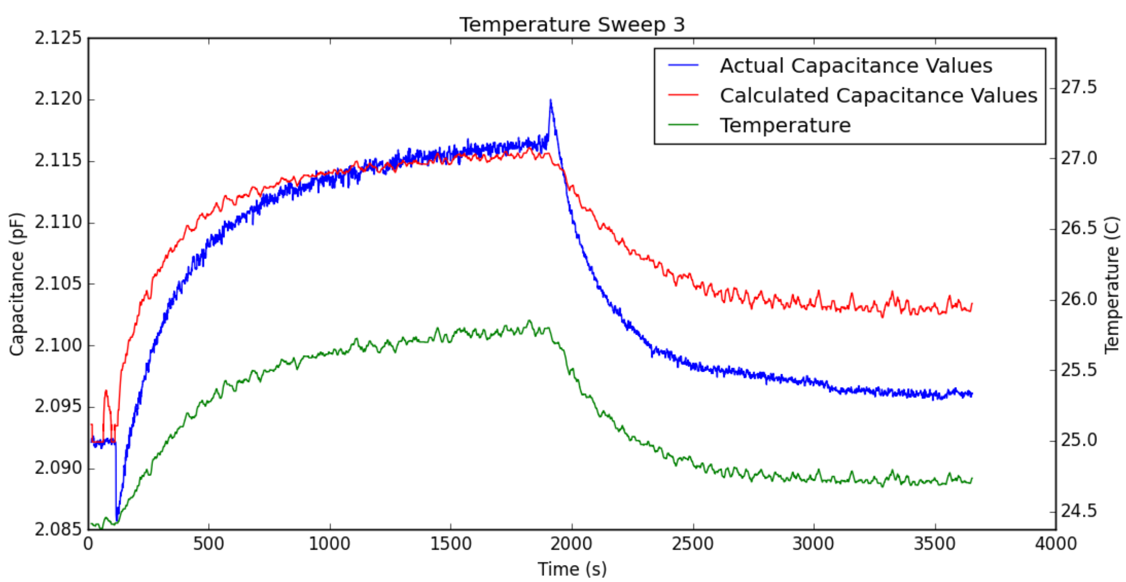

Figure 3.7: **Modeled capacitance change for trial 3.** Collected capacitance and temperature data plotted with modeled data for sweep 3. Figure generated by Matthew Francom.

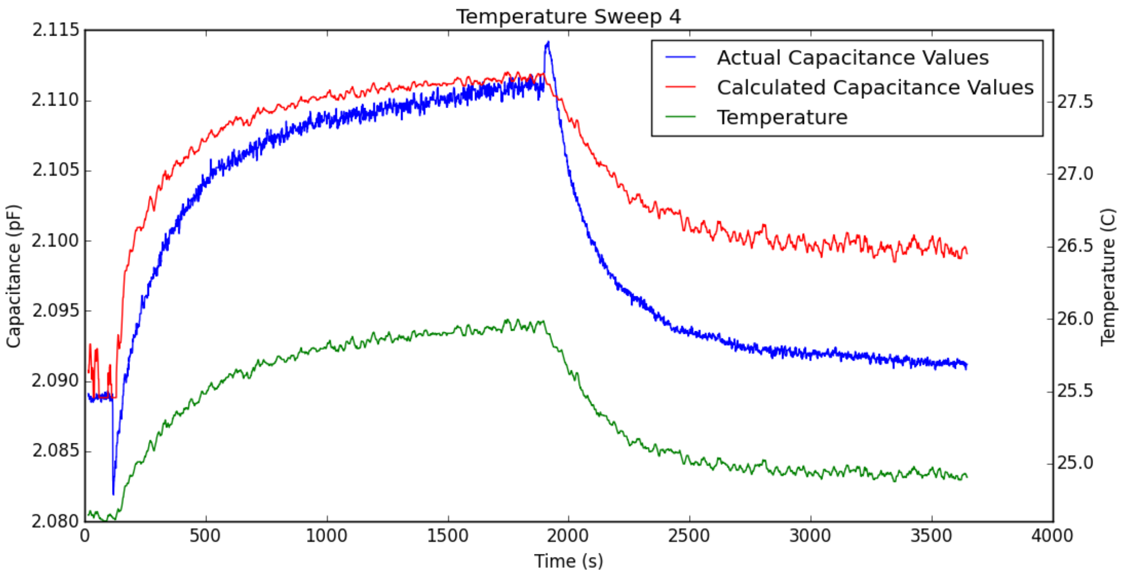

Figure 3.8: **Modeled capacitance change for trial 4.** Collected capacitance and temperature data plotted with modeled data for sweep 4. Figure generated by Matthew Francom.

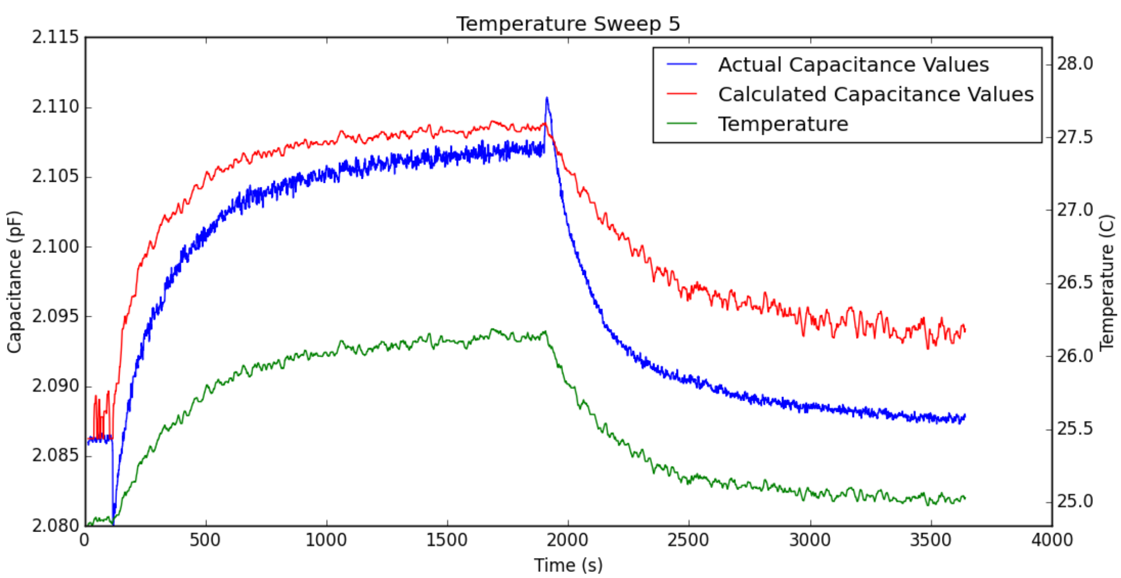

Figure 3.9: **Modeled capacitance change for trial 5.** Collected capacitance and temperature data plotted with modeled data for sweep 5. Figure generated by Matthew Francom.

These plots allow two key conclusions to be made about the capacitance manometers and the AD7747 detection circuitry. First, the capacitance manometer tracks the temperature changes during the heating cycle. Although it does not track the temperature with perfect accuracy, there is a max error of approximately 5 fF (as taken from temperature sweep 5). Assuming a conservative baseline capacitance of 2.086 pF and a capacitance change of approximately 19 fF, an error of 5 fF correlates to a 26.3% error relative to the capacitance change, but only a 0.240% error relative to the baseline capacitance.

Second, in this test arrangement the AD7747 chip is not good at tracking the temperature during the cooling cycles. When the test fixture is being heated with the ion gauges on, the primary source of heating is through radiation. Both the AD7747 chip and the capacitance manometer are in close proximity, so the heating should be fairly uniform between the two. When the ion gauges are turned off the fixture is dissipating heat, and the test fixture radiates heat as well as conducts heat away through the copper gasket and into the walls of the vacuum chamber. The manometer is mounted directly onto the glass slide which is mounted on the copper gasket and has a substantial amount of surface area in contact with the glass. The AD7747 chip is mounted onto the PCB break-out board and is only in contact with the glass slide through several wires and vacuum epoxy. Therefore the thermal sinks for the manometer and the AD7747 are quite different.

The inconsistencies between the actual capacitance and calculated capacitance present on the cooling cycles of all five sweeps are likely related to different heat dissipation. Evidence of this can be observed in all five sweeps at the end of each dataset, where the capacitance value tends to be near the baseline capacitance value of the beginning of each sweep, while the temperature measured by the AD7747 chip appears to be plateauing at a value above the baseline temperature value. No general conclusions can be made about the temperature measuring accuracy of the AD7747 chip because the dataset does not extend far enough in time, however the same anomaly is present in all five sweeps which indicates a consistent error present in the system.

3.3 Capacitance vs. Temperature Characterization (Second Iteration)

To test the theory that heating by the ion gauges are cause the valley and peak in the capacitance data, the vacuum chamber was modified by reorienting the ion gauges to prevent them from radiating directly towards the manometer. An image of the new ion gauge location is shown in Figure 3.10.

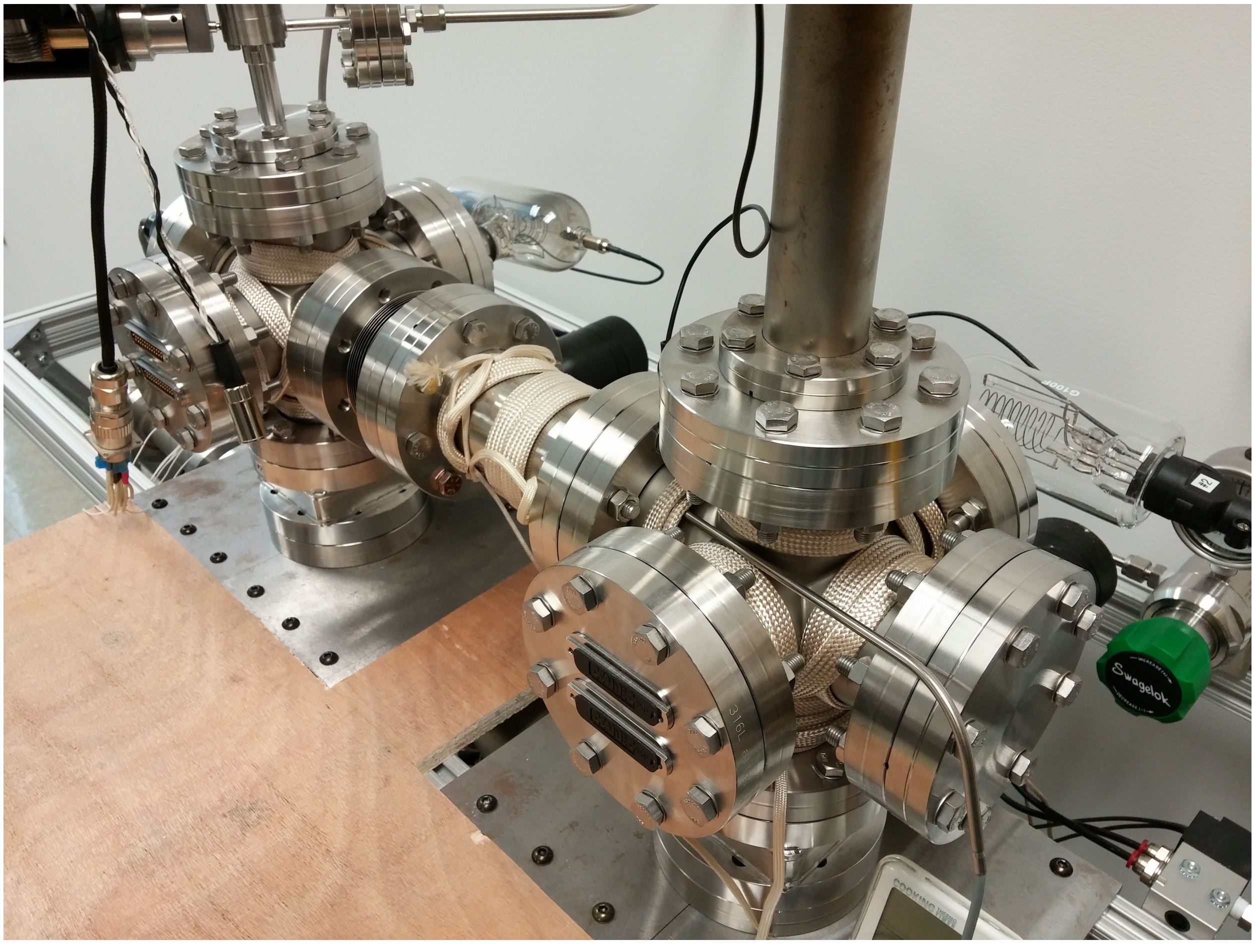

Figure 3.10: **Image of vacuum chamber with rear mounted ion gauges.**

3.3.1 Normalized Capacitance and Temperature Data (Second Iteration)

New sweeps were performed after reorienting the gauges. Similar to the previous temperature sweeps, there are 2 minutes of baseline capacitance and temperature data collection, 30 minutes of ion gauge heating, and 30 minutes of ion gauge cooling. Each temperature sweep is performed several days apart to allow adequate time for temperature equalization. The temperature data have similar bit resolution noise which is more prominent because the temperature swing is much lower in these sweeps. The capacitance and temperature data are again first passed through a median fit algorithm to eliminate all noisy outliers and are then passed through an eight-point moving average filter a total of ten times, and then normalized against their respective baseline values. The filtered and normalized datasets are shown in Figures 3.11 and 3.12, respectively.

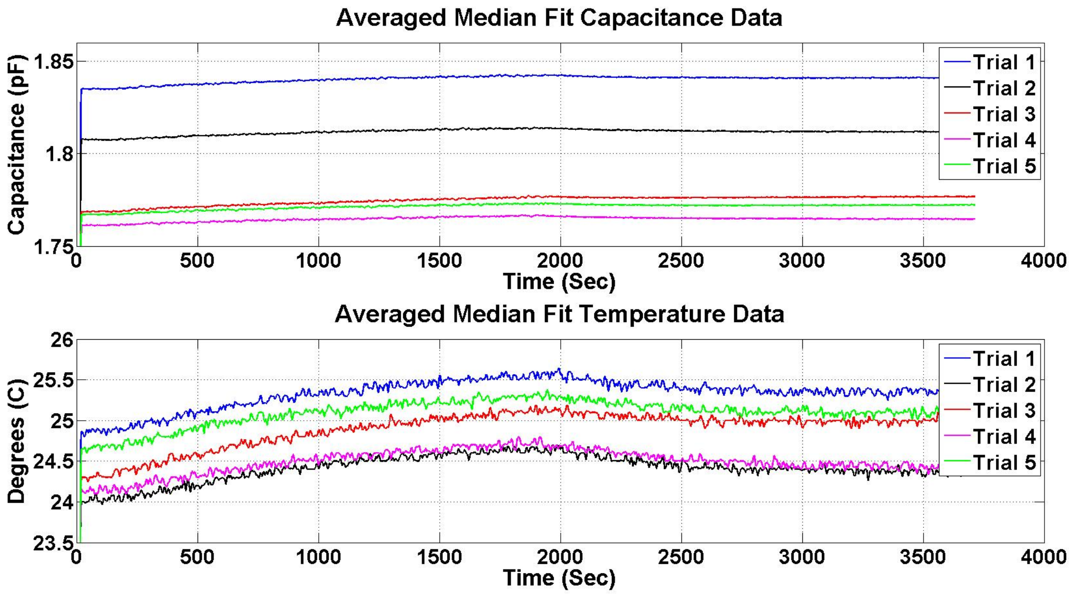

Figure 3.11: **Averaged and median fit temperature data (second iteration).** Median fit data passed through an averaging filter to minimize bit resolution distortion in the temperature data.

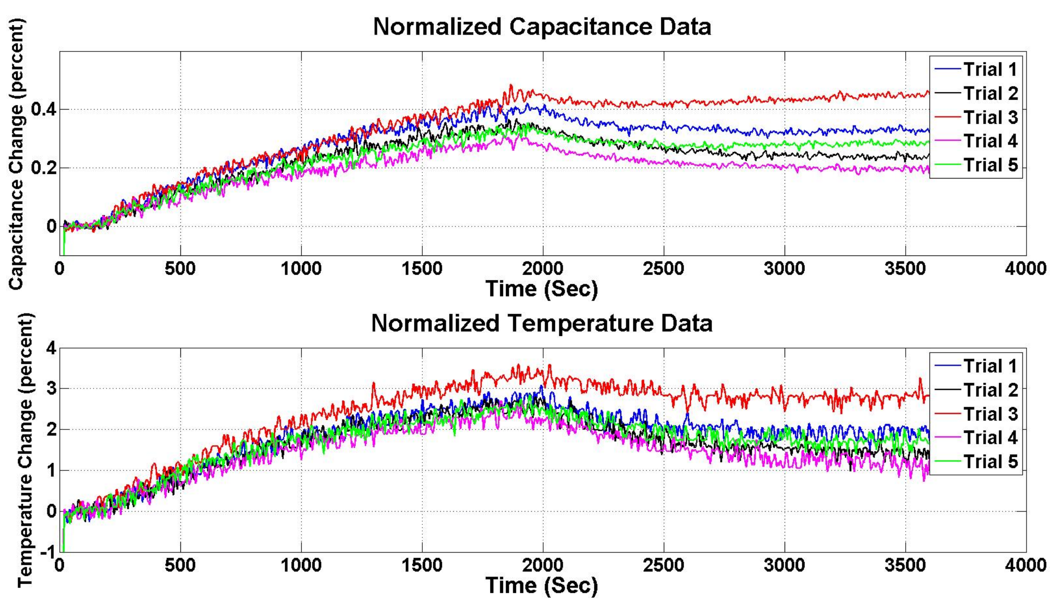

Figure 3.12: **Normalized temperature data (second iteration).** Normalized data for comparison of individual temperature sweep datasets.

The critical difference seen in this dataset is the loss of the valley and peak in the capacitance data. When the ion gauges are turned on and off there is no transient change in the capacitance data. Several similarities remain. The obvious similarity is the decreasing of the baseline capacitance with each sweep. Despite the reduction in baseline capacitance values, the pressure in the chamber was constant during all sweeps at 3.4 x 10^{-6} (10%) Torr. This opposes the conclusion that there is outgassing caused by the ion gauges. It should be noted that the fifth sweep actually has a higher baseline capacitance than the fourth sweep so the outgassing conclusion from the first iteration of the temperature sweeps is not definitive.

Compared to the first iteration temperature sweep dataset presented in Figure 3.2, this dataset seems to have a linear growth when the ion gauges are on, and very slow decay over the 30 minute period after the ion gauges have been turned off. This is a particularly odd behavior because there is no additional heat source on the test fixture causing the temperature to rise. This odd behavior echoes the anomaly present in the cooling portion of the previous iteration of temperature sweeps; however, this iteration of temperature sweeps seems to amplify the issue. The slow decay of the measured temperature when the ion gauges are turned off as well as the residual heat maintaining the measured temperature remain an anomaly.

3.3.2 Normalized Capacitance vs. Temperature Data (Second Iteration)

The normalized capacitance vs normalized temperature plot for the heating cycle is shown in Figure 3.13. The cooling cycle has been omitted as the data appear to be unreliable.

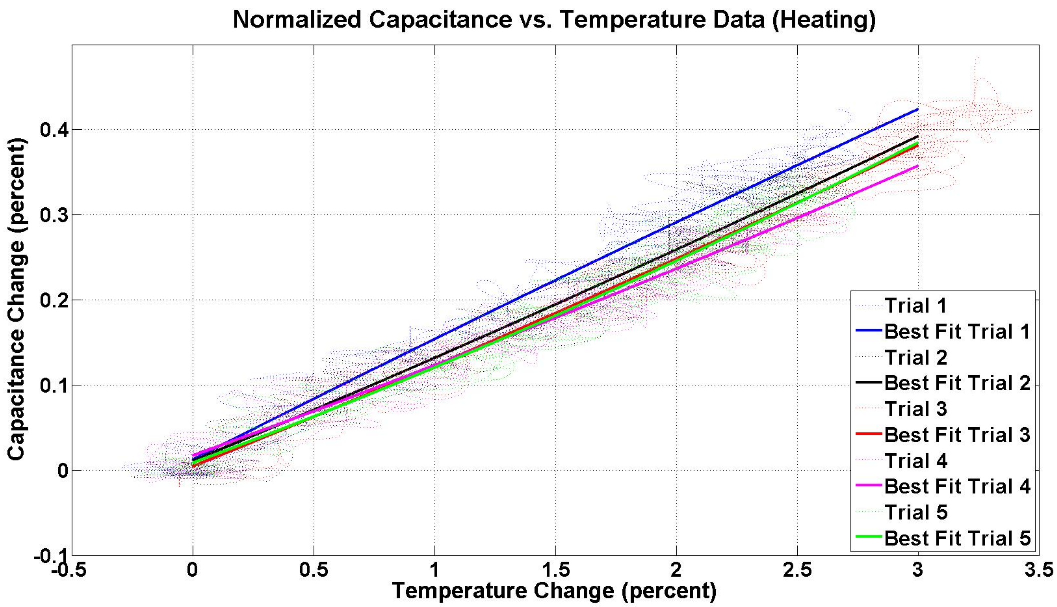

Figure 3.13: **Normalized capacitance vs. normalized temperature (second iteration, heating).** Normalized data for the heating cycles with ion gauges turned on. Best fit lines added for comparison.

When comparing the normalized capacitance to the normalized temperature in the reoriented ion gauge configuration (without direct radiative heat) the correlation is nearly linear. Additionally, all data points seem to be precise regardless of the baseline capacitance and temperature values, a characteristic that was not present in the previous iteration of temperature sweeps. The data from all sweeps is very tightly bound, allowing the conclusion that without radiative heat from the ion gauges, the capacitance manometer reacts predictably to temperature changes.

When comparing the second order polynomial best fit lines, Trials 2-5 all seem to be very close in slope, having very little influence from the second degree of the polynomial. Table 3.4 gives the coefficients for the polynomial best fit line given by the following equation.

$$f(x) = p1 * x^2 + p2 * x + p3 \tag{3.2}$$

Table 3.4: **Normalized capacitance vs. normalized temperature best fit coefficients (second iteration, heating).**

Trial	p1	p2	p3
1	-0.002155	0.1437	0.01235
2	0.00307	0.118	0.01075
3	0.003698	0.1147	0.004221
4	0.003768	0.1022	0.01701
5	0.006753	0.1052	0.008456

3.3.3 Comparison of First and Second Iteration Temperature Sweeps

A difference when comparing Figure 3.13 with the first iteration dataset presented in Figure 3.3 is the magnitude of the capacitance change. When comparing sweep number three (noted by the red color) from the temperature iterations in which the ion gauges provided direct radiative heat to the measurements made with the reoriented gauges, the percent capacitance changes corresponding to a 3% change in temperature are 0.634% and 0.4%, respectively.

This lower value when the manometer is heated indirectly, as well as the more linear relationship between the capacitance change and the temperature change, provide a reference that allow symptoms of another issue with the first iteration to become more clear. When the test fixture is heated with direct radiation from the ion gauge filament wire, the AD7747 chip and the manometer are not heating uniformly. The flexible membrane of the manometer is a reflective surface and the AD7747 chip is a black body IC. If radiation is the primary source of heat, then the two devices absorb heat at different rates. Conversely, when the two devices are not heated by radiation, as seen in the second temperature sweep iteration, the two devices appear to heat at a more uniform rate. As non-radiative heat is not always possible, a possible workaround would be to make the body of the AD7747 chip reflective to better mimic the surface of the manometers flexible membrane. By making the AD7747 chip reflective, the two devices would heat more uniformly and the resulting capacitance change vs temperature change might be more linear.

3.3.4 Measurement Chip Thermal Characterization

One critical component to the temperature data is the accuracy of the AD7747 measurement chip over the specified temperature ranges. As mentioned earlier the measurement chip has a bit resolution of 0.1° C. Additionally the measurement chip has an error of ±0.5° C when using the internal temperature sensor. Considering the temperature change seen in the first iteration trials was approximately 1.5° C, the error of the chip can be considered significant. However, the extensive filtering of the temperature data (seen in Figures 3.1 and 3.11) largely reduced the impact of the error. The AD7747 datasheet provides a plot (seen in Figure 3.14 below) that indicates the impact error may not be as severe considering the operating temperature was approximately 25° C for each temperature sweep.

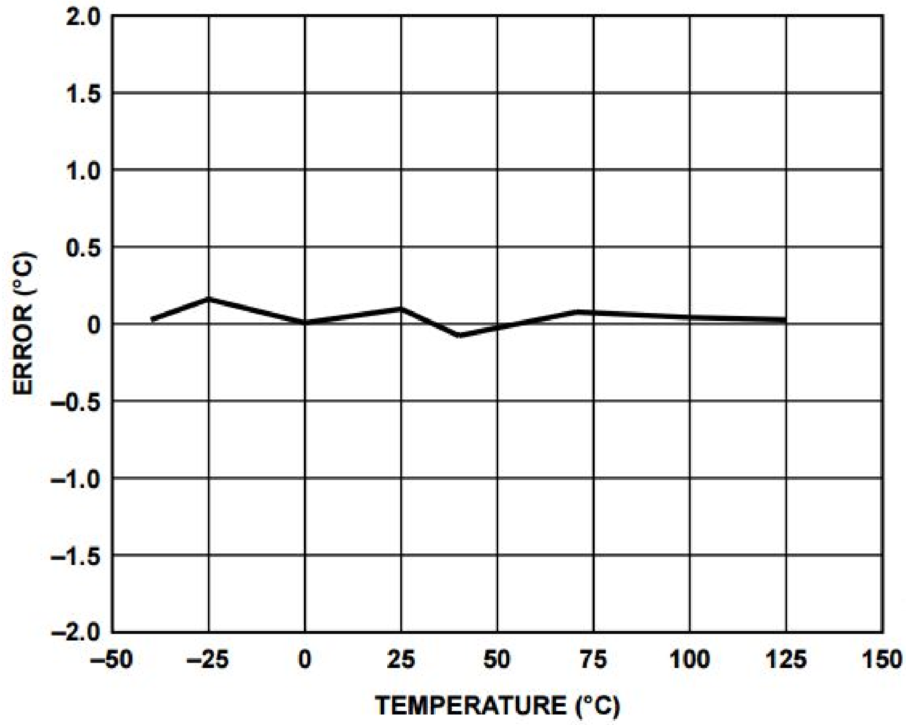

Figure 3.14: **AD7747 error plot.** Plot showing the expected error as a function of temperature (taken from AD7747 datasheet). Used under fair use, 2016. (Analog Devices, Inc.)

3.4 Capacitance vs. Differential Pressure Characterization

As mentioned earlier, the capacitance manometer has an expected capacitance change of 11 pF when a 7 x 10^{-6} Torr differential pressure is applied. An initial test procedure involving differential pressure steps was used to do preliminary characterization of the manometer. In this test, the leak valve was controlled to allow progressively larger differential pressures to be achieved over time. The testing began with very low differential pressures across the manometer, on the order of 1 x 10^{-8} Torr. This was increased by doubling the differential pressure of the previous step (i.e., differential pressure steps were 2 x 10^{-8}, 4 x 10^{-8}, 8 x 10^{-8}, 1.6 x 10^{-7}, 3.2 x 10^{-7}, etc.) until a differential pressure near 7 x 10^{-6} Torr was reached. Once the chamber had equalized at each pressure step, approximately 10 seconds were allowed to pass before moving onto the next pressure differential step. This would allow for any changes in the capacitance to have a distinct and well documented start and stopping point, to allow determination of the transient speed of the manometer as well as the settling time.

A second test procedure was used to check the validity of these results. Again, the testing began with a very low differential pressure on the order of 1 x 10^{-8} Torr and increased with only one large step to 3 x 10^{-6} Torr (this value was used because with large steps, there is some overshoot in the leak valve controller). Once a differential pressure of 3 x 10^{-6} Torr was achieved, a period of time of approximately 15 seconds was allowed to pass to determine the settling time of the manometer. By comparing these measurements, the settling time between the small differential pressure changes and the large pressure change can be directly compared.

3.4.1 Initial Results

Both test procedures, intended to provide initial characterization of the manometer, provided null results. The manometer showed no discernible capacitance change relative to the differential pressure despite the anticipated 11 pF change at 7 x 10^{-6} Torr. The only changes in capacitance were due to the inherent non periodic noise of the test fixture and AD7747 chip. Although not anticipated, this result provided some insight to the characteristics of the manometer, and suggested how the testing procedure needed to be modified. In consultations with the manometer fabrication team it was learned that the polyimide-based manometers are more robust than anticipated, and capable of withstanding differential pressures larger than values on the 10^{-2} Torr scale, and possibly as high as the 10^{0} scale, without tearing the flexible membrane. A new test procedure was subsequently devised to measure the capacitance manometer at larger differential pressures.

3.4.2 Changes to Chamber

The ion gauges are a limiting factor when trying to measure pressure differentials above 10^{-4} Torr. Ion gauges cannot be operated at 10^{-4} Torr and above; as mentioned earlier, a thermocouple is added to the left pressure chamber to allow the measurement of higher differential pressures. The medial equilibrium chamber connects the left and right pressure chambers. To prevent higher pressures in the left pressure chamber from affecting the right side, the solenoid gate valve is used to isolate the left pressure chamber from the medial equilibrium chamber. This effectively isolates the left pressure chamber from all other parts of the system, including the cryopump, allowing for large pressures to be achieved.

Unfortunately, one side effect is that the nitrogen leak valve can no longer be controlled via LabVIEW because the program uses the measurement from the left ion gauge to provide feedback on whether the leak valve should open or close. By not utilizing this gauge the LabVIEW program would not have the appropriate inputs and the leak valve would not function correctly. To obtain the high differential pressures, the leak valve is therefore controlled manually for the higher pressure tests. To prevent a runaway situation where the pressure increases too rapidly, the leak valve is slowly opened to allow a small leak in the system. Additionally, by closing the leak valve, securing the right ion gauge and cryopump, and re-aligning the left pressure chamber with the medial equilibrium chamber, the left pressure chamber can be brought back down to pressures on the order of 10^{-5} quickly to prevent tears in the capacitance manometer membrane. This re-equilization procedure was utilized at the end of each test sweep described below.

3.4.3 Differential Sweep Setup and Procedure

In order to characterize the capacitance manometers relationship to larger differential pressures, a revised test procedure is used. Tighter control on the start and end times is used to account for the discrepancies between sweeps (most notably from manually opening the leak valve, therefore having non-uniform leak rates between sweeps). All sweeps begin with the left ion gauge turned off, with differential pressure measured by the difference between readings from a thermocouple on the left pressure chamber and the right ion gauge. Pressure data for the left pressure chamber begins at 10^{-4} Torr and is allowed to increase until 0.3 Torr while the left pressure chamber remains at a constant pressure. The LabVIEW program is utilized only to capture the pressure data from the thermocouple and the right ion gauge. The AD7747 measurement chip GUI is utilized to capture the capacitance data.

A sweep begins after both gauges have been on for enough time to mitigate the temperature change discussed previously. After the appropriate amount of time has passed the AD7747 GUI begins capturing capacitance data. One minute later the LabVIEW program begins capturing data (this allows for both data sets to have a defined start time for aligning the data). After 30 seconds, the left ion gauge is turned off. After another 30 seconds the solenoid gate valve isolating the left pressure chamber from the medial equilibrium chamber is closed. At this point the leak valve is slowly opened until an increase in the thermocouple pressure is measured, at which point the leak valve is left in position. A consistent opening rate is sought; however, there are some discrepancies between each sweep. To account for this, the sweeps are all stopped at the closest minute once the thermocouple reaches 0.3 Torr.

3.5 Empirical Capacitance and Pressure vs. Time Data

The plots for the five differential pressure sweeps are shown in Figures 3.15 - 3.19. In the test fixture arrangement, the manometer is situated such that the differential pressure is separating the plates, causing the capacitance to decrease as the differential pressure increases. The trials shown were performed over the span of one month. All capacitance data have been filtered through a median fit algorithm to minimize noise and remove the effects of errant samples. For each sweep, the capacitance data and pressure data are shown on separate plots relative to time. Red vertical lines are used to show the start and stop of the relevant data. In addition to the capacitance data and differential pressure data, the right ion gauge pressure is shown on the same plot as the differential data.

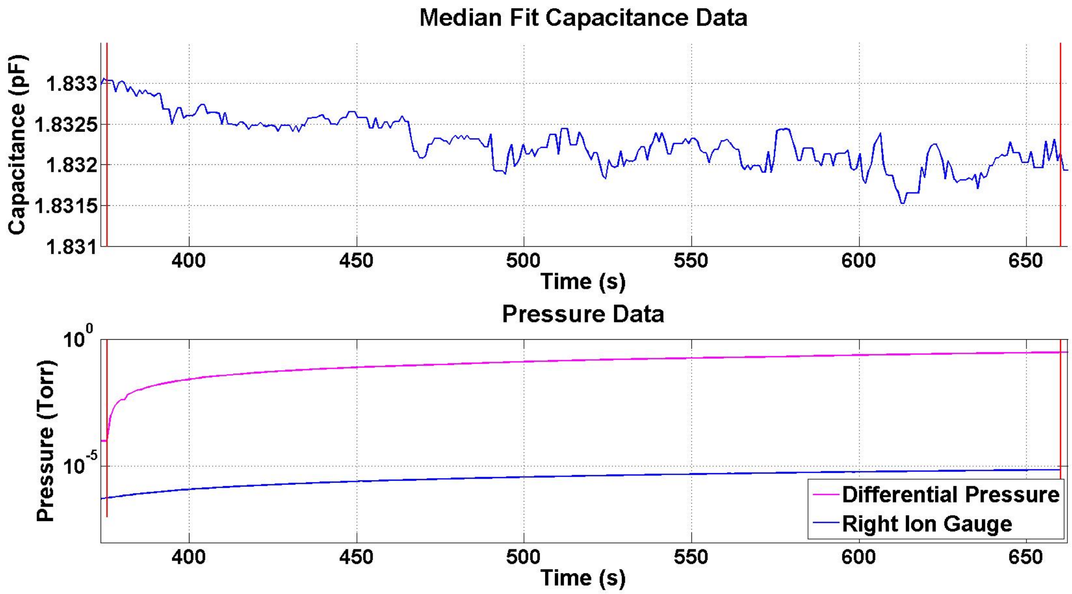

Figure 3.15: **Trial 1 of capacitance and differential pressure vs. time data.**

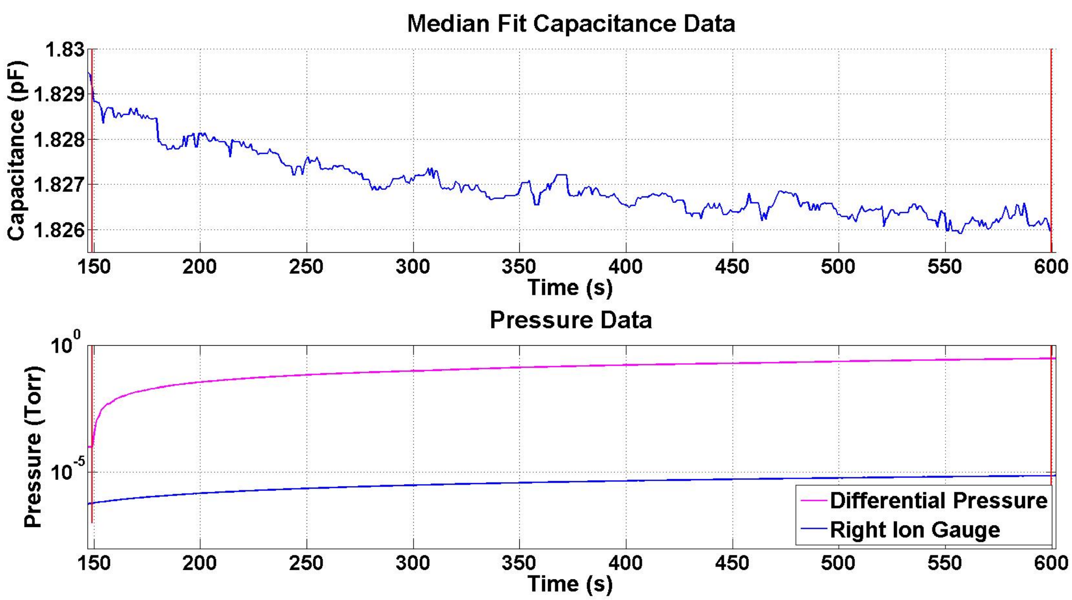

Figure 3.16: **Trial 2 of capacitance and differential pressure vs. time data.**

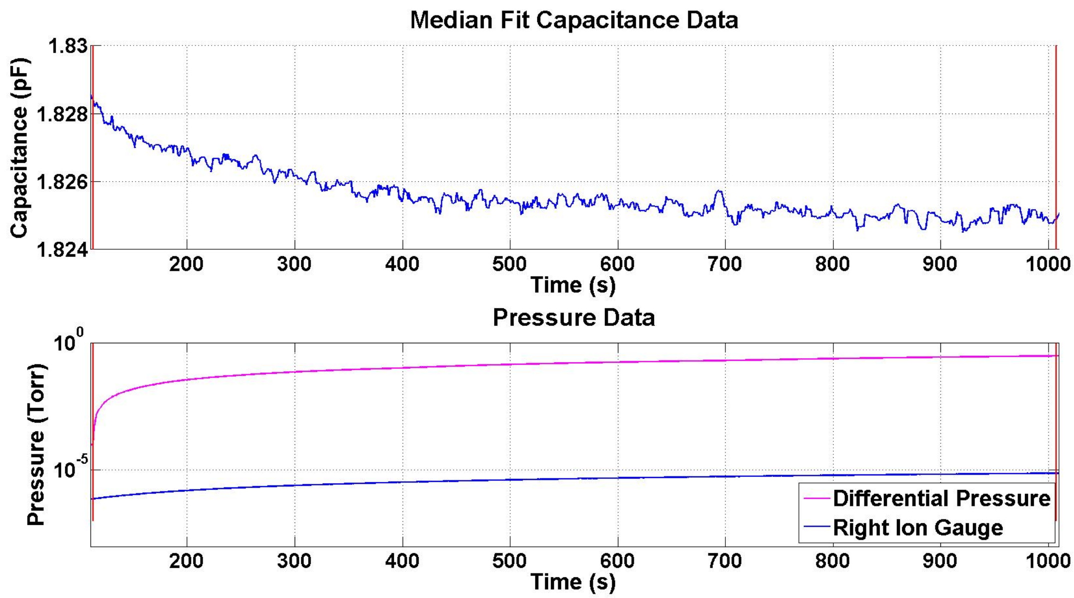

Figure 3.17: **Trial 3 of capacitance and differential pressure vs. time data.**

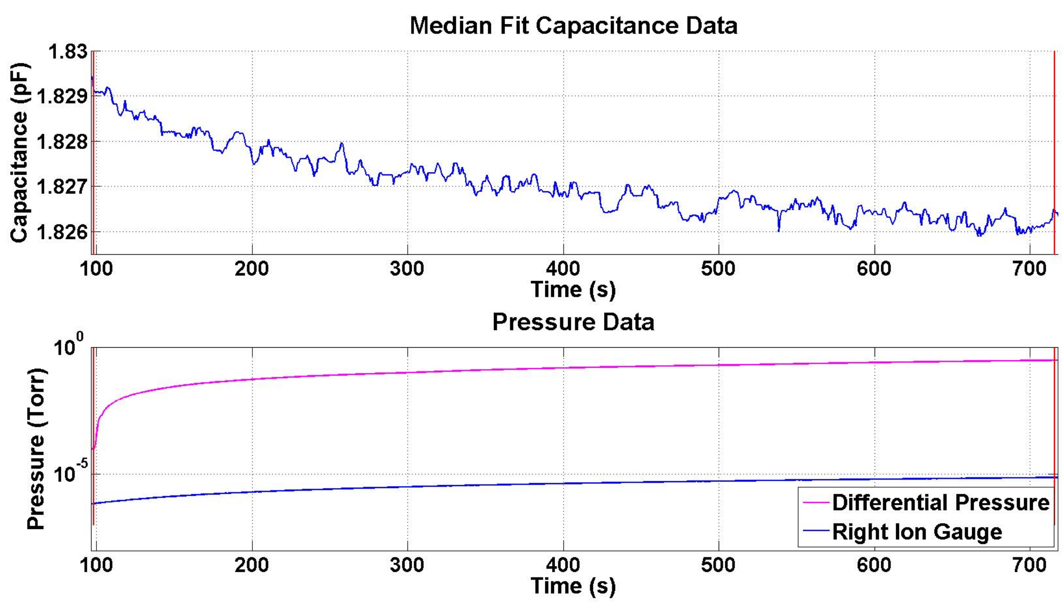

Figure 3.18: **Trial 4 of capacitance and differential pressure vs. time data.**

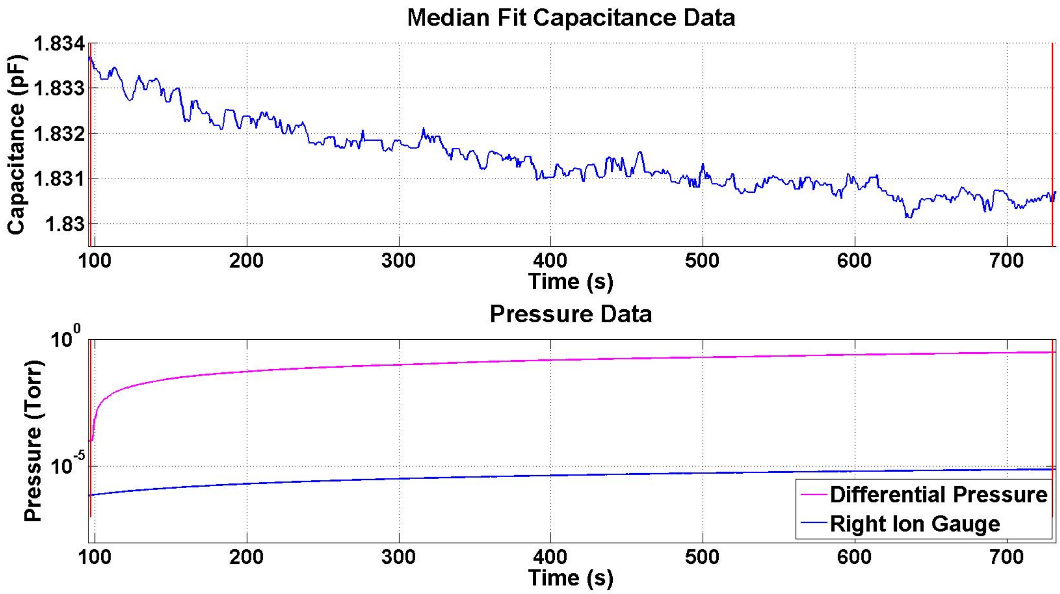

Figure 3.19: **Trial 5 of capacitance and differential pressure vs. time data.**

The initial impression from the plots above is that the manometer is functional and able to change when a differential pressure is applied. Sweeps 1 and 2 (Figures 3.15 and 3.16) seem to be less responsive than sweeps 3-5 (Figures 3.17, 3.18, 3.19), however the capacitance is decreasing as expected. The manometer output appears to be linearly related to the logarithmic scaled pressure differential, with the capacitance decreasing as the pressure differential increases. There are some differences between sweeps, however the capacitance data of each sweep seems to follow the same shape. To better see this, Figure 3.20 shows the normalized capacitance vs. the logarithmically scaled differential pressure. Power best fit functions are included in the plot for comparison.

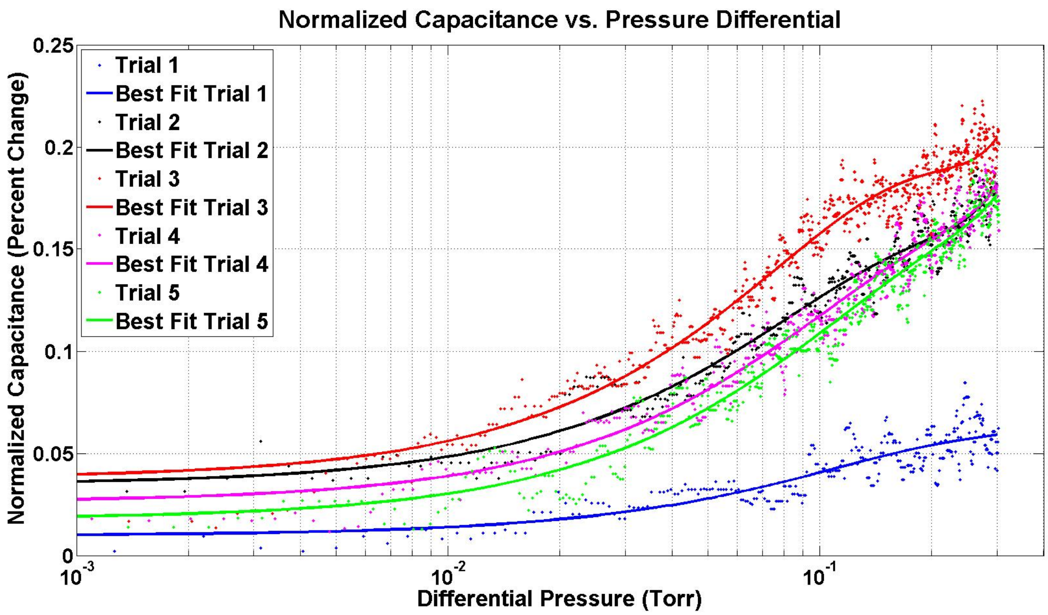

Figure 3.20: **Differential pressure vs. normalized capacitance.** Empirical data noted by data points with power function best fit lines included for comparison.

Trial 1 shows odd behavior, but trials 2-5 all have similar slopes and magnitudes. Ignoring the first trial and the lower portion of the pressure range, the data all show a similar variation in the capacitance change (percentage) over the logarithmically scaled differential pressure. There is some offset in the data, particularly in Trial 3, however the slopes of the best fit functions are all similar. Table 3.5 gives the coefficients for the cubic best fit function given by the following equation.

$$f(x) = p1 * x^3 + p2 * x^2 + p3 * x + p4 \tag{3.3}$$

Table 3.5: **Normalized capacitance vs. pressure differential best fit coefficients.**

Trial	p1	p2	p3	p4
1	1.5	-1.316	0.4246	0.009734
2	9.902	-6.081	1.424	0.03477
3	12.96	-8.388	1.906	0.03782
4	7.12	-4.831	1.323	0.02618
5	6.305	-4.42	1.288	0.01786

In testing over time at higher differential pressures, the capacitance manometer has a consistent capacitance change with respect to the differential pressure, and can be generally characterized with a first order polynomial function as it has a near linear dependence (a cubic function was used as it best characterizes the data over the tested differential pressure range). The offset can most likely be attributed to the length of time between trials and environmental changes that may have occurred over the period covering these experiments.

3.5.1 Notable Concerns with Empirical Data

Despite results showing a changing capacitance with respect to differential pressure, the data have several key problems to address. The first problem is the extremely small capacitance change. As expressed earlier, modelling work suggests that a change of 11 pF is expected at differential pressures near 7 x 10^{-6} Torr. In our experiments, trial 3 showed the largest change from the initial capacitance, but the change was only 3.5 fF at a differential pressure of 0.3 Torr. The capacitance manometer is therefore many orders of magnitude less sensitive than expected. The low level capacitance changes pose some threat to the validity of the measurements, since the capacitance data collected by the AD7747 measurement chip are near the noise level for the measuments. The AD7747 chip is only adding approximately .1% noise to the data (5.5 aF) which means the test fixture and other external factors are causing the noise in the measurements. With such a small measured capacitance, simple things such as changing proximity of signal wires in the vacuum chamber could cause a large enough capacitance to affect the data.

Another issue seen in Figures 3.15 - 3.19 is the rise in pressure of the right ion gauge as the differential pressure increases. The right pressure chamber is isolated from the rising pressure in the left pressure chamber through both the solenoid gate valve and the capacitance manometer test fixture. The manometer test fixture is the more likely source of the leak. The manometer may have some small tears that become larger when the flexible membrane is deflected, thereby allowing air to escape into the right pressure chamber. The consistency of the change across all five trials leads to some validity of this hypothesis, but without being able to view the capacitance manometer under a very high magnification it can not be confirmed.

Chapter 4

Conclusions and Future Work

4.1 Summary of Results

Our work has shown that the MEMS polyimide-based capacitance manometers are able to detect small temperature changes and large differential pressures. Data from Figure 3.13 show that when the capacitance manometer is heated, it has a linear relationship between the temperature and the capacitance change relative to the baseline, or initial, capacitance. Data from Figure 3.20 show that the capacitance manometer can also be characterized by a nearly linear relationship between the differential pressure (on a logarithmic scale) and the percent capacitance change relative to a baseline capacitance. Although the capacitance manometer is far less sensitive than expected, our study shows that a measurable capacitance change relative to differential pressures can be measured and unambiguously interpreted. We therefore conclude that these MEMS manometer hold some promise for low-power pressure measurements, but additional work is needed to mitigate the two main shortcomings of the devices revealed in our testing. Below we provide some suggestions for future development.

4.2 Future Work

4.2.1 Fabrication Issues

Although version 2 devices were deemed best for the testing reported here, it is noteworthy that the version 3 devices are a more elegant and appealing design (see Figures 2.1 - 2.3), since the measurement chip can potentially be mounted in close proximity to the manometer membrane. Future work should include a concerted effort to improve the solder pads for the measurement chip in the version 3 devices, in order to yield a single-board sensor with the shortest possible leads between the sensor and the measurement electronics.

It is also noteworthy that the number of manometers from which good capacitance measurements were obtained is far less than the number fabricated and delivered to VT for testing. This suggests that either more care is called for in handling and/or shipping the devices, or that a more carefully controlled process flow is required during fabrication to ensure that the devices have uniform characteristics. This is a common issue in semiconductor fabrication of new devices; it is often that case that many trials are required to establish a fabrication routine that yields good uniformity.

Solderability Issues

Specifically, further investigation of the solderability issue needs to be prioritized. Preliminary investigation has showed that soldering to a gold plated surface can severely inhibit the quality of solder joint, especially in applications where the gold plating is thicker than 0.75 μm. The gold plating on the manometer tested is 1.2 μm and can be viewed as a potential cause for the solderability issues. Typically, in thicker gold plating situations, the Au plating cannot disperse uniformly through the solder connection and becomes concentrated in areas, leading to degradation of the solder connection. Thinner gold plating needs to be investigated to see if this could aid in solving the solderability issue.

4.2.2 Addressing Sensitivity Issues

The primary problem keeping the manometer from meeting the specifications set forth in the project proposal is the lower-than-expected sensitivity of the capacitance manometer. The manometers built and tested in this project do not produce the large capacitance changes expected at low differential pressures. Additional MEMS fabrication work is necessary to mitigate the sensitivity issue. Simulations of the device geometry have identified a probable cause of the low sensitivity, as described below. These simulations suggest a path for improving the sensitivity of the manometer design.

The manometer is etched through a multistep procedure which is summarized Figure 4.1.

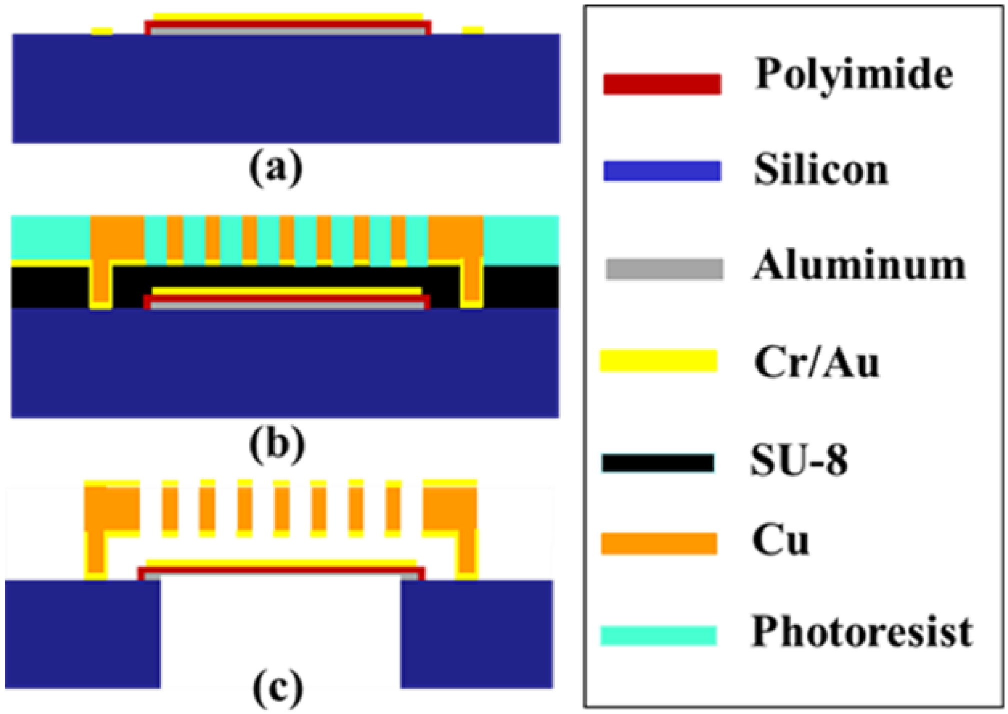

Figure 4.1: **Diagram of simplified MEMS process.** Diagram showing a simplified 2 step etching procedure to fabricate the capacitance manometers. Used with permission, 2015. (Lee, 2015).

Around the perimeter of the flexible membrane comprising the capacitance manometer are steep edges and sharp corners where the sacrificial layer could potentially remain after etching, as shown in Figure 4.2. Simulations were run to model how the sensitivity of the manometer would change if slight amounts of residue remain around the outer rim of the flexible membrane; these results are shown in Figure 4.3.

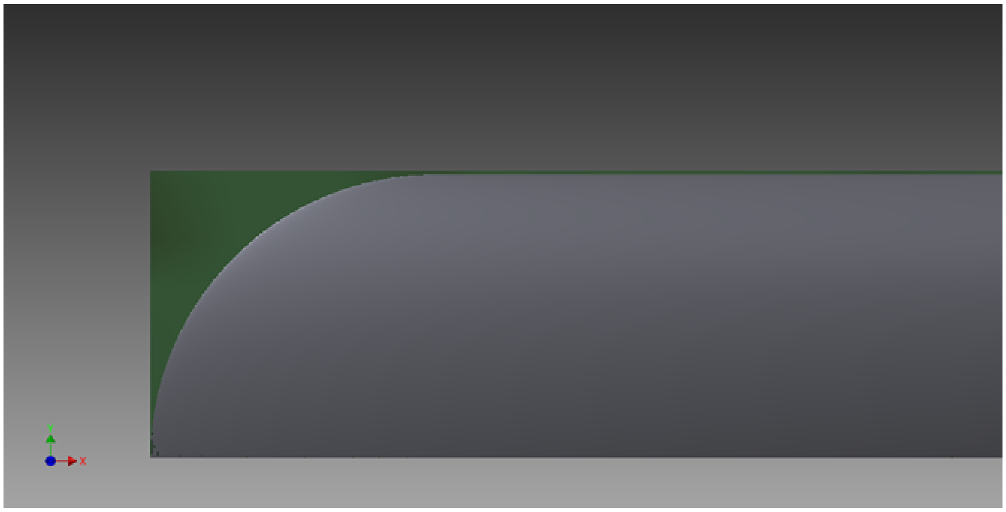

Figure 4.2: **CAD diagram of corner residue effect.** The green material indicates the shape and orientation of the corner residue effect, which may degrade the sensitivity of the manometers under test. Figure generated by Matthew Francom.

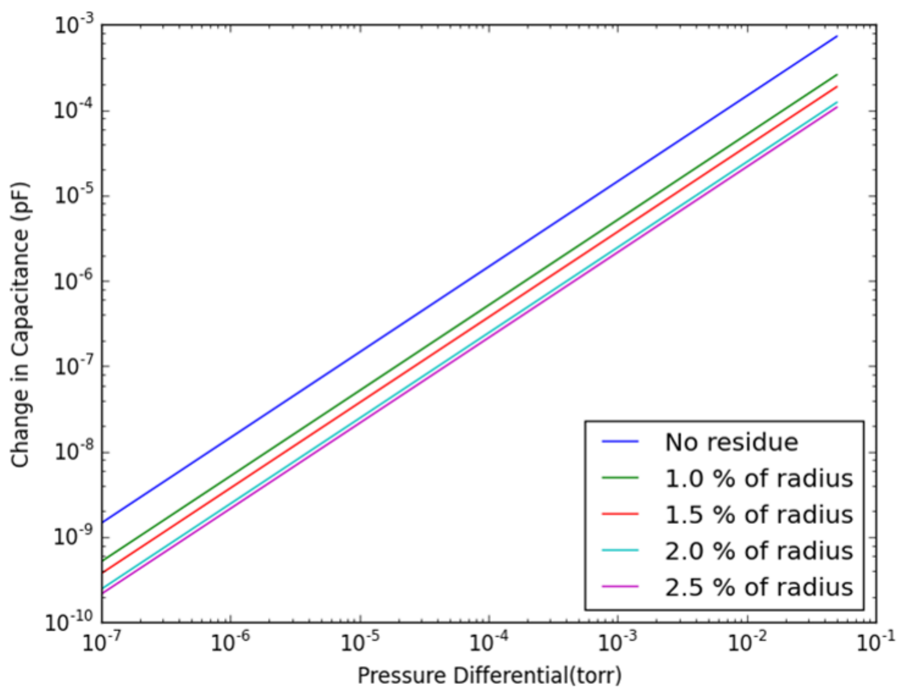

Figure 4.3: **ANSYS simulation showing sensitivity effect.** ANSYS simulation results showing the logarithmic pressure differential across the membrane for different amounts of residue around the perimeter of the etched region. Figure generated by Matthew Francom.

For comparison, Figure 4.4 shows the change in capacitance from the all five trials. The change in capacitance is calculated by multiplying the normalized percentage against the starting value. A power function is included as a best fit line for comparison. Table 4.1 gives the coefficients for the power best fit function given by the following equation.

$$f(x) = a * x^b + c \tag{4.1}$$

Table 4.1: **Capacitance change vs. pressure differential best fit coefficients.**

Trial	a	b	c
1	0.002089	0.2534	-0.0004207
2	0.005198	0.322	-0.000239
3	0.01155	0.09095	-0.006575
4	0.005767	0.337	-0.0005371
5	0.005923	0.395	-0.00042

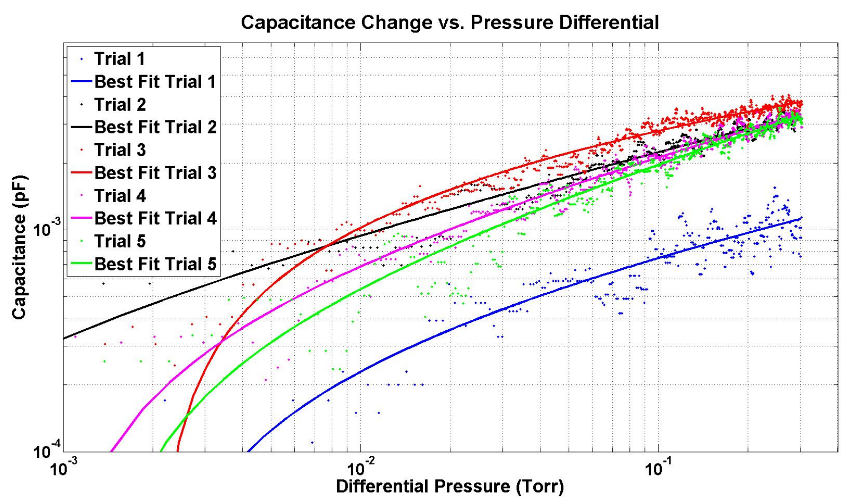

Figure 4.4: **Capacitance change vs. pressure differential.** Comparison of the actual capacitance change vs. the pressure differential for all five trials. Power best fit functions included for comparison

Although the information from the two plots can not easily be compared directly as the scales are substantially different, the lowering of the sensitivity with even 1% of the sacrificial layer remaining is concerning, as this is certainly possible during the fabrication process. Without viewing the manometer under strong magnification, it is difficult to conclude this as the culprit of the sensitivity issues. Moving forward, the remaining material on the capacitance manometer is an important factor to consider when determining the sensitivity of the device.

4.2.3 Addressing the Ruggedness of Devices

After the capacitance manometers were fabricated, they all measured between 7-14 pF by LCR meter testing performed at UTD. Upon arrival at Virginia Tech, the same manometers provided the measurements given in Table 2.1. These measurements included manometers that had been shipped by an overnight shipping company as well as manometers that were hand delivered. The manometers are extremely sensitive to shock and vibration, even though they are rugged enough to withstand large pressure differentials. It appears that transporting them introduces considerable changes to their baseline characteristics. Future work should therefore address the durability of the manometers to ensure that the devices can withstand the stresses of shipment.

It may be possible to fabricate support structures between the membranes and the grid electrode to make the devices robust during shipping and launch, as long as a method for removing the supports prior to testing can be developed. Possibilities include supports that could be burned off prior to use by passing a large current between the flexible membrane and the grid (through the support structure), or fabricating the supports out of a material that would rapidly be removed in vacuum when exposed to a particular gas (such as atomic oxygen in LEO environments). Future work should also include modifying the etching process during fabrication to reduce or eliminate the edge residue effect, which should improve the sensitivity of the MEMS devices.

Bibliography

Analog Devices, Inc. (2007). *24-Bit Capacitance-to-Digital Converter with Temperature Sensor* (C ed.). Analog Devices, Inc.

Bulwith, R. A. *Soldering to Gold - A Practical Guide*. Accessed April 21, 2016. www.solderworld.net/docs/soldering-to-gold.pdf.

Crump, D. (2013). *Capacitor Manometer Differential Pressure Test Chamber User Manual*. M.Eng. Project and Report, Virginia Tech

Earle, G. D. and J. B. Lee. Development of a Robust Low-Power Pressure Transducer for Thermospheric Applications. NASA proposal.

Kurt J. Lesker Company. *Global Vacuum Product Guide*. www.lesker.com. 9th Edition.

Lee, J. B. (2015, October). Manometer fab and simulation write-up v1. Email correspondence.

Lee, J. B. (2016, April). Capacitance manometer questions. Email correspondence.

Appendix A

Median Fit MATLAB Code

```
function [medfitresult, samples] = MedFit(dataset, N, OverlapSize)

%% NOT FOR DISTRIBUTION
% Created by: Cameron Orr
% Created on: Sept. 28, 2015


% Inputs
%   dataset - the Data that will have the median fit algorithm applied.
%
%   N - the number of points on either side of the current point that are
%   included in the median calculation.
%
%   OverlapSize - the number of steps between each median point calculation.
%   For best results use a value less than N.
%
%
% Outputs
%   medfitresult - the array of values created by doing a median fit of the
%   input dataset.
%
%   samples - array of time samples with the same index lenght as
%   medfitresult.



d = size(dataset);
n = 1;
temp = zeros(2*N+1,1);

count = n+N;
medfitresult = zeros(d);
```

```
while count < (d(:,1)-N)

    for n1 = 0:N
        temp((N+1)+n1) = dataset(count+n1);
        temp((N+1)-n1) = dataset(count-n1);
    end

    temp = sort(temp);

    medfitresult(n) = temp((N+1),1);

    count = count + OverlapSize;
    n = n+1;
end

i1 = find(medfitresult, 1, 'first');
i2 = find(medfitresult, 1, 'last');

medfitresult = medfitresult(i1:i2);

samples = transpose(1:n-1);
```